OPEN ACCESS
International Journal of Neural Systems, Vol. 36, No. 7 (2026) 2650018 (30 pages)
© The Author(s)
DOI: 10.1142/S0129065726500188

World Scientific
www.worldscientific.com

Int. J. Neur. Syst. 2026.36. Downloaded from www.worldscientific.com
by 84.118.51.191 on 05/04/26. Re-use and distribution is strictly not permitted, except for Open Access articles.

A Feasibility Study of Navigating Emotional States Using Real-Time Representational Similarity Analysis fMRI Neurofeedback

Xuelei Wang [*], Assunta Ciarlo [†,‡], Michael Lührs [†,‡], Alexander Atanasyan [§], David Böken [§], Jürgen Roßmann [§], Michael Schluse [§], Maren Jäger [*], Marisa Nordt [¶,‖], Fengyu Cong [**,††,‡‡], Klaus Mathiak [*,§§], David E. J. Linden [¶¶], Rainer Goebel [†,‡], David M. A. Mehler [*,‖‖,***,†††,§§§] and Jana Zweerings [*,‡‡‡,§§§]

[*]*Department of Psychiatry, Psychotherapy and Psychosomatics, Medical School RWTH Aachen University, Aachen, Germany*

[†]*Brain Innovation B.V., Maastricht, The Netherlands*

[‡]*Department of Cognitive Neuroscience, Faculty of Psychology and Neuroscience Maastricht University, Maastricht, The Netherlands*

[§]*Institute of Man-Machine Interaction, Faculty of Electrical Engineering and Information Technology RWTH Aachen University, Aachen, Germany*

[¶]*Department of Child and Adolescent Psychiatry, Psychosomatics and Psychotherapy Medical Faculty RWTH Aachen University, Aachen, Germany*

[‖]*JARA-Brain Institute II, Molecular Neuroscience and Neuroimaging RWTH Aachen and Research Centre Juelich, Juelich, Germany*

[**]*School of Biomedical Engineering, Faculty of Medicine Dalian University of Technology, Dalian, P. R. China*

[††]*Faculty of Information Technology, University of Jyvaskyla, Jyvaskyla, Finland*

[‡‡]*Key Laboratory of Social Computing and Cognitive Intelligence, Ministry of Education Dalian University of Technology, Dalian, P. R. China*

[§§]*JARA-Translational Brain Medicine, RWTH Aachen University, Aachen, Germany*

[¶¶]*Mental Health and Neuroscience Research Institute Faculty of Health, Medicine and Life Sciences Maastricht University, Maastricht, The Netherlands*

[‖‖]*Institute of Translational Psychiatry, Medical Faculty University of Münster, Münster, Germany*

[***]*School of Psychology, Cardiff University Brain Research Imaging Center (CUBRIC) Cardiff University, Cardiff, UK*

[†††]*dmehler@ukaachen.de*

[‡‡‡]*jzweerings@ukaachen.de*

Received 17 November 2025
Accepted 19 January 2026
Published Online 16 March 2026

[§§§]Corresponding authors.

This is an Open Access article published by World Scientific Publishing Company. It is distributed under the terms of the Creative Commons Attribution 4.0 (CC BY) License, which permits use, distribution and reproduction in any medium, provided the original work is properly cited.

Real-time functional magnetic resonance imaging neurofeedback (rt-fMRI-NF) is a promising noninvasive brain computer interface (BCI) technique for enhancing self-regulation of affective brain states. However, conventional univariate rt-fMRI-NF approaches struggle to discriminate distributed neural patterns underlying distinct emotions. This study implemented an rt-fMRI semantic neurofeedback (rt-fMRI-sNF) paradigm incorporating real-time representational similarity analysis (rt-RSA) to enable navigation among emotional states. Four emotion-specific base patterns were first derived from functional localizer runs and then used as target patterns during neurofeedback. Using an RSA-informed circular semantic map (CSM), participants received real-time visual feedback indicating both the similarity and intensity of their current brain activity relative to target patterns. Participants were instructed to use mental imagery to shift their brain activity toward the specific target pattern and enhance its intensity. Analyses of localizer data revealed overlapping regional activations across emotions and demonstrated that RSA reliably distinguished between emotional states. Group-level mixed-effects modeling of neurofeedback performance indicated significant within-run improvements and higher initial performance in the second run. Together, these results demonstrate the methodological feasibility of an RSA-informed rt-fMRI-NF framework for multivariate brain-state modulation and establish a foundation for future studies examining its transferability and clinical relevance.

Keywords: Real-time fMRI neurofeedback; representational similarity analysis; multivariate pattern decoding; emotional regulation.

Int. J. Neur. Syst. 2026.36. Downloaded from www.worldscientific.com
by 84.118.51.191 on 05/04/26. Re-use and distribution is strictly not permitted, except for Open Access articles.

1. Introduction

Real-time functional magnetic resonance imaging neurofeedback (rt-fMRI-NF) has emerged as a promising technique for enabling individuals to learn self-regulating their own brain activity.[1,2] Among its various applications, emotion regulation is one of the most extensively studied domains.[3] A growing body of research supports the feasibility of rt-fMRI-NF in modulating affective states[4,5] and demonstrates its clinical promise in modulating brain activity[6] and symptoms in psychiatric conditions such as depression,[7,8] posttraumatic stress disorder (PTSD)[9–11] and attention deficit hyperactivity disorder (ADHD).[12,13]

Traditional rt-fMRI-NF paradigms typically employ a univariate analysis approach, where feedback is based on the average activation level within a predefined brain region and often visualized using a thermometer-like display.[14] However, this approach has limited ability to distinguish between different mental processes that involve the same brain region, which is a major challenge for emotion regulation because previous studies have shown that different emotions often activate overlapping brain regions.[15,16] This challenge has motivated a broader shift toward multivariate pattern-based approaches for decoding affective states across neuroimaging modalities. In the electroencephalography (EEG) literature, distributed emotional representations have been successfully decoded using advanced machine-learning frameworks, including subject-aware transformers and interactive Gaussian process models.[17,18] In fMRI research, multivariate approaches use multivoxel pattern analysis to differentiate between distinct neural activation patterns,[19,20] enhancing the capacity of rt-fMRI-NF to target and regulate multiple emotional states.

Building on the advantages of multivariate statistics, one promising method that has gained increasing attention in fMRI research is representational similarity analysis (RSA).[21,22] Unlike traditional activation-based analyses, RSA quantifies the relationships between mental representations by examining the representational geometry of neural activation patterns, thereby enabling finer differentiation between closely related cognitive or emotional states. Previous applications of RSA to fMRI data investigated a variety of cognitive processes, including action control,[23] visual object perception[24,25] and emotion representation across sensory modalities.[26] In the context of rt-fMRI-NF, a promising real-time RSA application to conduct RSA-informed neurofeedback, known as real-time fMRI semantic neurofeedback (rt-fMRI-sNF), has been introduced[27,28] and evaluated[29,30] using visual mental imagery tasks. These proof-of-concept studies demonstrated that participants were able to use mental imagery strategies to generate and modulate semantic representations of objects corresponding to external objective sensory stimuli. Applying a similar approach to emotion regulation-based neurofeedback

Int. J. Neur. Syst. 2026.36. Downloaded from www.worldscientific.com
by 84.118.51.191 on 05/04/26. Re-use and distribution is strictly not permitted, except for Open Access articles.

would open new avenues for more personalized self-regulation training and potentially clinical applications.[31] However, whether it is feasible to effectively adapt rt-fMRI-sNF to mental imagery of affective states remains to be demonstrated.

A key aspect in rt-fMRI-sNF is the format in which visual feedback is presented to neurofeedback users. Traditional thermometer-like displays only have one degree of freedom and only reflect the overall (e.g. mean-field) intensity of activation within a target region. Thereby, they cannot provide additional information about the relationship (e.g. representational distance) between distinct neural/voxel patterns under different experimental conditions. To overcome this limitation, previous rt-fMRI-sNF studies[29,30] have introduced a two-dimensional semantic map, which is produced by multi-dimensional scaling (MDS) such that the participant's current mental state is projected as a moving dot. Specifically, the location of the moving dot is determined by the similarity between the participant's current voxel pattern (e.g. evoked by mental imagery) and a target voxel pattern (e.g. determined by localizer runs). A semantic map hence allows participants to see how closely their brain activity matches a target mental state. To further enhance the visual feedback information, a novel visualization method was proposed to incorporate both pattern similarity and pattern intensity in a so-called circular semantic map (CSM).[31,32] The CSM combines multiple thermometers in a circular arrangement—each indicating the activation intensity of a specific neural pattern—with a dynamic arrow showing the direction of change in pattern similarity. This hybrid form of visual feedback captures two critical aspects of neural representation, highlighting its potential usability in rt-fMRI-sNF.

Building on the first rt-fMRI-sNF implementations applied to object imagination with similarity-only feedback,[29,30] this study extends this emerging framework to the more complex domain of emotional mental imagery and introduces a dual-dimensional feedback visualization that conveys both the similarity and intensity of brain activity. To our knowledge, this work provides the first demonstration of RSA-based neurofeedback for internally generated affective states using multi-metric CSM feedback. Specifically, this study aimed to investigate:

(i) the effectiveness of RSA-based multivariate analysis in distinguishing between multiple emotional states evoked through mental imagery obtained during the localizer scans;
(ii) the feasibility and efficacy of applying the rt-fMRI-sNF paradigm for emotion regulation;
(iii) the usability and potential of navigating brain activity via the CSM-based visual feedback.

2. Materials and methods

2.1. *Participants*

A total of 27 healthy individuals (21 females), aged (mean ± standard deviation (SD)) 28.7 ± 8.3 years, with normal or corrected-to-normal vision and without acute severe neurological, psychiatric, or somatic disorders took part in the main study. A separate pilot group of 6 healthy participants was recruited to assess the experimental design and the usability of task instructions. Data from the pilot group was only used for design validation and excluded from all subsequent analyses. Prior to the scanning session, participants provided written informed consent, and the study was approved by the local ethics committee [EK 23-175].

Since this work was designed as a feasibility study, no formal *a priori* power analysis was conducted; instead, sample size was determined based on practical constraints and the goal of evaluating methodological feasibility.[33]

2.2. *Experimental design*

This feasibility study was preregistered (https://osf.io/5ybuw). Participants were instructed to engage in four emotional states through mental imagery (joyful relaxation, sadness, enthusiasm and anger) during four sequential functional localizer scans, respectively (Fig. 1(a)). The selection of these four emotional states was based on the valence and arousal model[34] and informed by a previously published investigation.[35] Specifically, two positive and two negative emotions with matched arousal levels (high

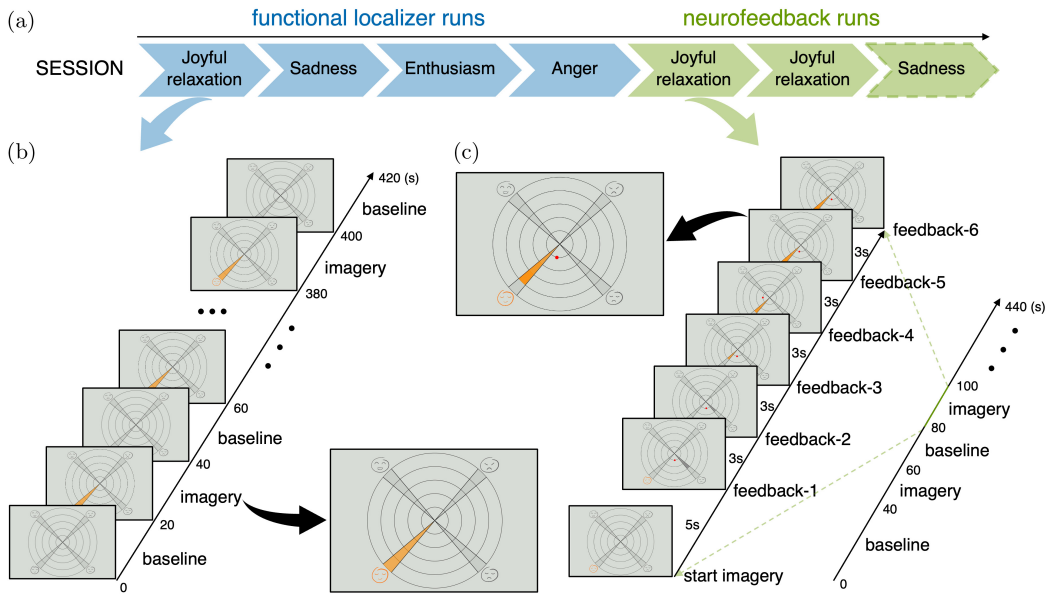

Fig. 1. (Color online) Experimental design. (a) Illustrates the sequence of measurements with four functional localizer runs (blue) and two neurofeedback runs having joyful relaxation as target emotion (green). A third neurofeedback run targeting sadness was optional, and hence, not performed by all participants. (b) Shows the condition sequence within a localizer run for the example of joyful relaxation, with interleaved baseline and imagery blocks. The emotion icon and thermometer (colored in orange during the localizer imagery block) were used as visual cues to prompt participants to perform mental imagery of the corresponding emotion. (c) Shows the condition sequence within a neurofeedback run and one of the mental imagery blocks in detail (exemplified for the emotion of joyful relaxation). During the neurofeedback run, participants were instructed to engage in mental imagery once the emotion icon was highlighted in orange. After 5 s, the feedback display was initiated and prompted by a red dot (which indicated the similarity of the current activity pattern with respect to the target pattern) and orange thermometer wedges (which indicated the intensity of the current activity pattern). The three other emotional states that were not targeted during the neurofeedback run were displayed in gray. During each mental imagery block, the feedback display was updated every three seconds, resulting in six trials per imagery block.

and low) were selected according to the classification probability of a machine learning model on the valence and arousal ratings of different emotions.[35] To deliver instruction and feedback information to the participants, a CSM was used,[31] which consisted of four thermometers, each corresponding to a specific emotion. Schematic facial icons were used in the CSM to minimize additional perceptual and semantic processing while preserving intuitive emotional cues. Prior to scanning, participants were informed about the experimental procedure and received standardized task instructions. They were then asked to use mental imagery to separately induce and intensify each of the four emotional states based on their own subjective experience, without receiving any specific imagery instructions beforehand. Subsequently, they reported on a scale from 1 to 10 if they managed to induce the emotional state, how familiar they were with each specific emotion, as well as their perceived valence and arousal levels. In addition, participants were asked to indicate where in the body they sense the emotion. Prior to and after the measurement, all participants completed questionnaires assessing their current mood state and their ability to regulate emotions, as measured by the Profile Of Mood States (POMS)[36] and Emotion Regulation Questionnaire (ERQ).[37] At the end of each neurofeedback run, participants were asked to report, on a scale from 0 to 10, the extent to which they were able to induce the target emotion, how well they were able to control their brain activity based on the feedback, and what strategies they used. To enhance the documentation of the study design and reporting, the "Consensus on the reporting and experimental design of clinical and cognitive-behavioral neurofeedback studies (CRED-nf checklist)" is enclosed[38] (see Appendix B).

Int. J. Neur. Syst. 2026.36. Downloaded from www.worldscientific.com
by 84.118.51.191 on 05/04/26. Re-use and distribution is strictly not permitted, except for Open Access articles.

Int. J. Neur. Syst. 2026.36. Downloaded from www.worldscientific.com
by 84.118.51.191 on 05/04/26. Re-use and distribution is strictly not permitted, except for Open Access articles.

2.2.1. *Functional localizer runs*

The acquisition of an anatomical T1-weighted MRI scan preceded four functional localizer runs (one for each emotion). The functional localizer runs were used to define each participant's individual target region and to generate the corresponding emotion-specific base patterns. Each run contained 10 emotion imagery blocks interleaved with 11 baseline blocks, both lasting 20 s (Fig. 1(b)). Participants were requested to perform the mental imagery task when the icon of a specific emotion and the corresponding thermometer turned orange on the CSM (imagery blocks), and to count backwards from 100 when all emotion icons turned gray (baseline blocks). After completion of the four localizer runs, RSA was used to select voxels with high discernibility between four distinct emotions. The blood-oxygen-level-dependent (BOLD) signal from the selected target voxels served to generate feedback signals throughout the neurofeedback training.

2.2.2. *Neurofeedback runs*

The experimental design of neurofeedback runs was like that of functional localizer runs, except the initial baseline block was extended to 40 s to account for potential preprocessing delays and to stabilize the online statistic computation (Fig. 1(c)). Participants were instructed to imagine one preselected emotion during each of the ten imagery blocks of the neurofeedback runs. The visual feedback provided information to the participants about two key aspects. First, the wedges of the target emotion thermometer were dynamically filled based on the intensity of the current brain activity pattern relative to the corresponding base pattern, extracted during the localizer runs. Second, the current activity pattern was represented as a moving red dot projected onto the CSM. The participants had to adjust their imagery strategy to move the red dot as close as possible to the target emotion, and to increase the target thermometer level.

2.3. *Data acquisition*

MR imaging data were acquired with a 3.0 Tesla Siemens MAGNETOM Prisma whole-body MRI system (Siemens Medical Solutions, Erlangen, Germany), equipped with a 20-channel head coil. A T1-weighted magnetization-prepared rapid gradient-echo (MPRAGE) sequence was acquired for each participant at the beginning of the scanning session and used as anatomical reference (acquisition matrix: 256×256, time of repetition (TR): 2000 ms, echo time (TE): 3.03 ms, 1 mm isotropic voxels, flip-angle: 9°, 176 sagittal slices, duration: 4.3 min).

Functional localizer and neurofeedback runs consisted of 420 and 440 volumes, respectively. A multi-band multi-echo echo-planar imaging (EPI) sequence with the following parameters was used for the data acquisition in each functional imaging run: acquisition matrix: 64×64, TR: 1000 ms, TE: [13, 27.8, 42.6, 57.4 ms], flip-angle: 67°, 36 transverse slices per volume that were acquired in interleaved order, inter-slice gap: 0.75 mm, voxel size: $3 \times 3 \times 3$ mm, multi-band factor: 3, GRAPPA factor: 2. Partial Fourier acquisition was used with a 7/8 phase-encoding factor to reduce acquisition time.

Data were transferred in real-time from the image reconstruction computer to an analysis workstation for real-time fMRI processing using a direct transmission control protocol/internet protocol (TCP/IP) connection.

2.4. *Online analysis*

Data were processed online using Turbo-BrainVoyager (TBV) version 4.2 (Brain Innovation B.V., Maastricht, The Netherlands) and imported in Python (3.6.12) using the TBV Network Access Plugin and the corresponding interface (https://github.com/expyriment/expyriment-stash) as part of the open-source Expyriment library 0.10.0.[39] The rt-RSA Python tool, freely available at https://github.com/assuntaciarlo/rtRSA_GUI, was used for pattern analysis and feedback display.

Based on previous studies,[40,41] a set of emotion-related brain regions was defined, generating a corresponding volume of interest (VOI) in Montreal Neurological Institute (MNI) space. The VOI included cortical regions based on the Schaefer atlas (17-network parcellation, 200 parcels, 1 mm resolution)[42] and subcortical regions based on the Harvard-Oxford atlas (maximum probability maps, thresholded at 25%, 1 mm resolution).[43] The resulting mask covers a wide range of known emotion-related cortical and subcortical structures and was primarily used to reduce computational load and ensure stable real-time performance, rather than to

Int. J. Neur. Syst. 2026.36. Downloaded from www.worldscientific.com
by 84.118.51.191 on 05/04/26. Re-use and distribution is strictly not permitted, except for Open Access articles.

restrict the analysis to a small set of regions. The list of regions in the VOI can be found in Table A.1.

The online analysis pipeline began by combining multi-echo images using per-volume T2*-weighted sum,[44,45] followed by real-time data preprocessing and statistical modeling in TBV. The preprocessing steps included motion correction with trilinear interpolation and intra-session alignment (to the first volume of the first functional run) and spatial smoothing with a 6 mm full width at half-maximum (FWHM) Gaussian kernel. The statistical modeling was based on a voxel-wise recursive least squares general linear model (GLM) which was incrementally computed with one predictor for the imagery task, six motion parameters and a linear confound predictor. At the end of each localizer run, TBV performed an offline voxel-wise GLM on the whole time series to extract the stimulus-specific t-map associated with the contrast "task versus rest". After all the four localizer runs, the rt-RSA tool was used to generate four base patterns by selecting voxels which were related to emotion imagination (univariate selection) and allowed semantic discernibility between emotions (multivariate selection). In the univariate selection, voxels were picked based on their absolute t-values, specifically those whose absolute t-values ranked within the top 60% to 90% of all the voxels within the defined emotion network. The multivariate selection first used a searchlight approach (with a spherical radius of 1 voxel) to generate a four-by-four representational dissimilarity matrix (RDM) for each voxel of the initial mask obtained from the univariate selection. This RDM encoded the dissimilarities between the four emotional patterns obtained from each searchlight, defined as one minus Pearson's correlation coefficient. Voxels were then selected if their RDMs achieved the top 5% similarity to a predefined model RDM, which treated emotions of opposing valence as maximally dissimilar while disregarding differences in arousal. Specifically, in the model RDM, the dissimilarity is set to 2 between positive and negative emotions (joyful relaxation versus sadness or anger, and enthusiasm versus sadness or anger), and 0 between emotions of the same valence (joyful relaxation versus enthusiasm, and sadness versus anger). The percentage thresholds and the model RDM were determined using the pilot dataset ($N = 6$), during which several parameter combinations were heuristically evaluated to achieve stable and robust real-time performance across participants. The selected parameter set was then fixed and applied consistently in the main study ($N = 27$). Voxel sets were used to construct four emotion-specific base patterns which then served as fixed comparison references across all neurofeedback runs.

During each neurofeedback run, the same preprocessing and statistical modeling steps were performed via TBV. In addition, the current brain activity pattern within the defined target region was correlated with respective base patterns. The correlation results were then used to calculate the location of the red dot and thermometer level.[32] The red dot was plotted between the thermometer representing the emotion with the highest correlation value and its neighboring thermometer (the one with the next higher correlation). The angular distance ratio of the red dot to the highest correlated emotion thermometer was calculated by the following formula:

$$\text{distance_ratio} = 1 - \frac{\text{highest_corr}}{\text{highest_corr} + \text{neighbor_corr}}.$$

The final location of the red dot was determined by multiplying the distance ratio by the angle between the highest correlated thermometer and its neighboring thermometer. The highest correlated emotion thermometer was filled according to the pattern intensity level and the filling color was orange for the target emotion or gray for nontarget emotions. To compute the intensity level, the current activity pattern vector was first projected on the highest correlated base pattern vector. The relative length of the projected vector to the base pattern vector was then referred to as the normalized intensity level. The corresponding thermometer was filled by converting the intensity level into one of five levels, each corresponding to a fixed increment of 0.2.

2.5. *Offline analysis*

The offline MRI data preprocessing was performed using HeuDiConv v1.3.2[46] and fMRIPrep v24.1.1 (ignored susceptibility distortion correction and slice timing correction; normalized to MNI152NLin2009-cAsym, with 2 mm resolution).[47,48] The following analysis, statistical tests and plotting relied on TBV

Int. J. Neur. Syst. 2026.36. Downloaded from www.worldscientific.com
by 84.118.51.191 on 05/04/26. Re-use and distribution is strictly not permitted, except for Open Access articles.

and Python packages, including NumPy 1.19.2,[49] Pandas 1.1.5,[50] SciPy 1.5.2,[51] Statsmodels 0.12.2,[52] Nilearn 0.9.2,[53] NiBabel 4.0.2,[54] Matplotlib 3.3.4.[55] and Seaborn 0.11.2[56] The offline analysis scripts can be found at https://github.com/xuelei-1021/rsanf.

To control for multiple comparisons across analyses, different correction procedures were applied depending on the analytical framework. Univariate activation analyses were corrected at the cluster level using Monte Carlo simulations for both first- and second-level models (initial cluster forming threshold $p < 0.01$, cluster-level threshold $p < 0.05$). Region-level comparisons across emotions were corrected using false discovery rate (FDR) correction across regions ($p < 0.05$). For block-wise neurofeedback performance comparisons, p-values were Bonferroni-corrected for the number of runs ($n = 2$). In individual-level neurofeedback analyses, statistical significance of performance slopes was assessed using FDR correction across metrics ($p < 0.05$). When applicable, the Shapiro–Wilk test was used to assess normality and guide the choice between parametric and nonparametric tests ($p < 0.05$).

2.5.1. *Neural activity analyses*

Brain activity patterns during emotion imagery from both univariate and multivariate perspectives were examined. Univariate analyses assessed traditional task-related BOLD responses using a "task versus rest" contrast, while RSA-based multivariate analyses characterized distributed voxel patterns and representational dissimilarities between emotions.

Univariate activation analyses

The first-level analysis was performed using the FirstLevelModel module in Nilearn (0.9.2), implementing a voxel-wise GLM with high-pass temporal filtering (128 s cutoff, cosine basis functions), hemodynamic response function (HRF) modeling from Statistical Parametric Mapping (SPM), time series standardization, spatial smoothing with a 6 mm FWHM Gaussian kernel, and autoregressive (AR(1)) noise modeling. The GLM model was fitted to the time-series data to estimate participant- and stimulus-specific effects (beta values), including the predictors of interest for task and rest conditions, as well as confound predictors derived from fMRIPrep (six motion parameters, motion outliers, physiological parameters from cerebrospinal fluid, white matter and the top five components for anatomical component correction[57]). The "task versus rest" contrast computation produced a z-score map, indicating how strongly the BOLD signal differs between the imagery and baseline blocks for each participant and stimulus. Each resulting z-map was first thresholded at the voxel level and then corrected for multiple comparisons at the cluster level to estimate the cluster size threshold. The subsequent second-level analysis was conducted using the SecondLevelModel module in Nilearn (0.9.2). Based on the individual z-score maps from the first-level analysis, a one-sample t-test was applied for each stimulus across all participants. The resulting contrast t-maps were also cluster-level corrected.

To explore the sensitivity of different brain regions to multiple emotions, 39 regions which showed more than 50% overlap with the predefined VOI (see Table A.2), based on the automatic anatomical labeling (AAL) atlas,[58] were selected for further analysis. The individual z-score map was averaged within different regions of interest (ROIs) and then analyzed across participants. The mean value, SD and distribution were computed across all participants for each ROI and stimulus. Paired t-tests or Wilcoxon signed-rank tests, depending on the distribution normality, were performed within each ROI between different emotions. The resulting statistics were then corrected across all the ROIs.

Multivariate activation analyses

Based on real-time output data, voxel selection distributions were first examined, including selecting frequency across participants and regional selection proportion. The selecting frequency was calculated across individuals after projecting selected voxels onto the standard MNI152 template. The region-level selection proportion was defined as the fraction of selected voxels within each ROI relative to the total selected voxels. These proportion values were then averaged across participants and ranked across regions for visualization.

Pairwise dissimilarities between emotions were then quantified using group-level RDM and its 95% confidence intervals. Derived from the online RDM, dissimilarity values were first converted back to correlation coefficients and transformed using Fisher's z-transformation. The transformed values were

averaged to obtain the mean, and the SD was used to calculate the 95% confidence intervals for z-scores. The mean z-score and its confidence interval bounds were then inversely transformed to obtain Pearson's r correlation values. Finally, the mean RDM and its confidence intervals were derived by subtracting the corresponding correlation values from 1.

2.5.2. *Neurofeedback performance evaluation*

Neurofeedback performance was quantified using three complementary metrics capturing different aspects of participants' regulation behavior. Pattern similarity was measured as the Pearson's correlation between the current brain activity pattern and the target base pattern, providing an implicit measure of neural (dis)similarity. In addition, two metrics were presented directly to participants via the CSM: angular distance, which quantified the directional deviation between the moving red dot and the target emotion icon as a spatial measure of regulation accuracy, and intensity level, which represented the normalized projection strength of the current activity pattern onto the target base pattern and was visualized as the height of the corresponding emotion thermometer. The intensity metric used in the offline analysis was defined to be greater than zero only when the current pattern showed the highest similarity to the target base pattern, thereby ensuring that intensity feedback reflected selective engagement of the intended emotional state.

Group-level evaluation was first conducted over the entire feedback time sequence. The mean and 95% confidence interval of each performance metric across participants were calculated. Specifically for Pearson's correlation, values relative to all nontarget base patterns were also computed. Learning effects within and between runs were examined using linear mixed-effects models (LMMs) implemented in the python function Statsmodels (0.12.2). The first two feedback time points were excluded while fitting the model to avoid low initial values caused by limited data. The model included run, time, and their interaction as fixed effects, with participant as a random intercept. To interpret the significance of the fixed effects within both runs separately, the model was fit twice, each time changing the reference level of the run term. Intercept and linear slope differences between runs were extracted to reflect variations in initial performance and learning rate, respectively. To account for potential nonlinearity (e.g. performance plateaus toward the end of a run), additional exploratory models incorporating quadratic or exponential time terms were fit and compared using a likelihood ratio test (LRT).

Group-level neurofeedback performance was also evaluated by comparing each metric between the initial and final feedback block (based on the median value across six feedback time points within the block). The statistical significance was tested via paired t-tests or Wilcoxon signed-rank tests, depending on distribution normality, and then corrected using Bonferroni for two comparisons.

Individual performance evaluation involved two parts: computing a neurofeedback score for each participant and run, and examining its relationship with participants' perceived control ratings. Neurofeedback scores were obtained by fitting a linear regression model to each metric's values over time. Regulation was considered successful for a given metric if the score showed a statistically significant improvement over time. Participants' perceived control ratings, reported on a scale from 0 to 10, reflected their subjective sense of control over brain activity during neurofeedback. To characterize the distribution of the ratings, the mean and SD across participants were calculated for each run, and a paired t-test was conducted to compare ratings between runs. Depending on the distribution normality, either Pearson's or Spearman's correlation was used to assess the relationship between objective neurofeedback scores (i.e. coefficients of the linear regression model) and subjective perceived control ratings.

Furthermore, to visualize individual self-regulation processes, the MDS algorithm[59,60] was applied to the four base patterns to estimate a two-dimensional representational space for each participant. The real-time neurofeedback patterns were then projected into the same space and displayed as continuous points, reflecting participants' learning trajectories.

Additionally, participants provided subjective reports related to their emotion imagery after each run. These included brief ratings of their experienced emotional state as well as descriptions of the imagery strategies they used during the task. Reported imagery strategies were classified into three categories: autobiographical memory recall, imagined situations

Int. J. Neur. Syst. 2026.36. Downloaded from www.worldscientific.com
by 84.118.51.191 on 05/04/26. Re-use and distribution is strictly not permitted, except for Open Access articles.

Int. J. Neur. Syst. 2026.36. Downloaded from www.worldscientific.com
by 84.118.51.191 on 05/04/26. Re-use and distribution is strictly not permitted, except for Open Access articles.

(i.e. events that did not actually occur or were fictional), and body-related sensations (i.e. awareness of current breathing or bodily feelings). Subjective emotion ratings were analyzed descriptively by computing the mean and SD across participants for each run, with the aim of characterizing the overall distribution of experienced emotional states rather than serving as a primary outcome measure.

3. Results

All participants ($N = 27$) completed four localizer runs. Most of them ($N = 24$) completed two neurofeedback runs targeting joyful relaxation, while one participant completed only one such run. Two participants did not complete any neurofeedback runs due to scanner-related technical issues ($N = 1$) or personal scheduling conflicts ($N = 1$). Approximately half ($N = 14$) of the participants additionally performed an optional neurofeedback run targeting sadness.

3.1. *Analyses of the localizer data*

3.1.1. *Univariate activations*

The results of the group-level univariate analysis for the localizer data are summarized in Fig. 2 (see Fig. A.1 for the corresponding analysis for the neurofeedback data). Significant activation clusters, based on the "task versus rest" contrast, were consistently observed across conditions in the prefrontal cortex (PFC; Fig. 2(a)). This activation pattern appears to be consistent with regions typically engaged in emotion imagery and processing.

In the ROI analysis based on averaged z-values, no significant differences emerged between conditions. This result indicates that simply considering the average activity within each region, as typically assessed in univariate analysis, was insufficient to distinguish between the considered emotions. Results for the 10 ROIs showing the highest group-level activity across conditions in the left hemisphere are illustrated in Fig. 2(b) (see Fig. A.2 for all 39 ROIs). While there was a trend to differentiate positive and negative emotions in dorsolateral superior frontal gyrus (dlSFG) and middle frontal gyrus (MFG), no region showed significant differences. This finding highlights the limitation of univariate analysis in recognizing the neural fingerprints of distinct emotions.

3.1.2. *RSA patterns*

The distribution of selected voxels was examined at both voxel and region levels. At the voxel level, the spatial pattern of selected voxels during the online analysis (Fig. 3(a)) closely matched the offline group-level t-maps (Fig. 2(a)). At the ROI level, the regions with the highest selection proportion (Fig. 3(b)) largely overlapped with those showing the strongest activation in the univariate analysis (Fig. 2(b)), primarily involving the frontal gyrus and anterior cingulate cortex (ACC). Based on the base patterns derived from these selected voxels, the group-level averaged RDM distinguished the four target emotions, most prominently along the valence dimension (Fig. 3(c)). A similar pattern could also be observed in the lower and upper bounds of the 95% confidence interval, indicating the robustness of the valence-specific distinctions. Overall, the multivariate results demonstrated the potential of this approach for reliably separating the considered emotional states.

3.2. *Neurofeedback performance*

Here, the neurofeedback performance analyses for the emotion of joyful relaxation were reported, as it was completed by the majority of participants in two consecutive runs, allowing for both within-run and between-run performance comparisons. Analysis of the optional third neurofeedback run targeting sadness, which was performed by fewer participants and included a single run, is provided in Figs. A.3–A.5 and Table A.3.

3.2.1. *Group-level neurofeedback performance*

Full run time-sequence analysis

The neurofeedback performance curves of three metrics over feedback time points are illustrated in Fig. 4. In Fig. 4(a), Pearson's correlation coefficients between the real-time brain pattern and each of the four emotional base patterns are plotted at every feedback time point, providing a dynamic view of how closely participants' neural activity aligned with each target state. The correlation with the target

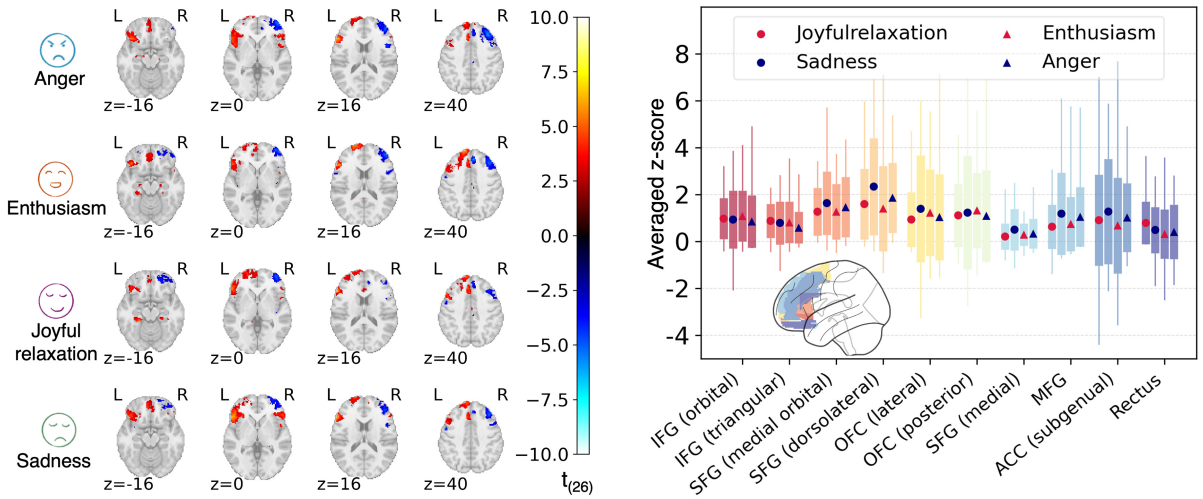

(a) (b)

Fig. 2. (Color online) Univariate patterns based on the raw localizer data. (a) T-maps of significant activation for each condition (task versus rest) in MNI space (voxel-level thresholded at $p < 0.01$, cluster-level corrected at $p < 0.05$). Only clusters encompassing the target VOI are shown. (b) ROI analysis (left hemisphere), computed by averaging the individual z-maps within each ROI. The boxplot summarizes the mean, SD and distribution of averaged z-scores across participants. The color and shape of each node represent the valence and arousal dimensions of the emotions (circular shape=low arousal, triangular shape = high arousal; red=positive emotions, blue=negative emotions). No region showed significant differences (i.e. $p > 0.05$) between high and low arousal emotions, or between different positive and negative emotions.

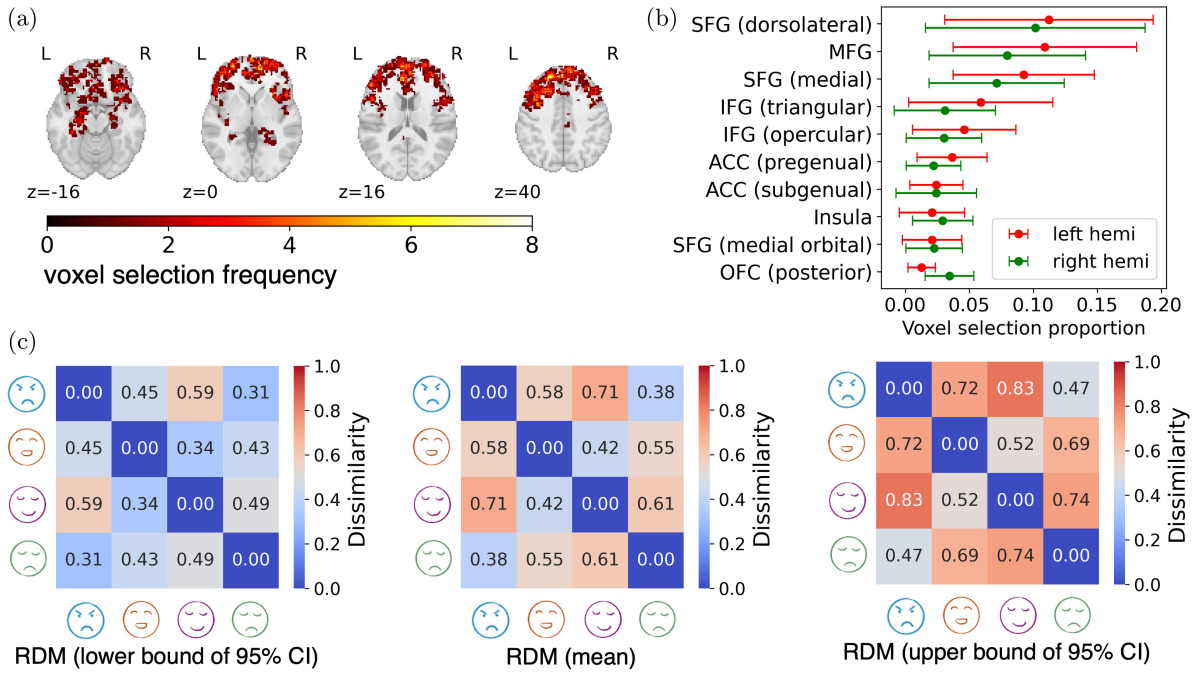

Fig. 3. (Color online) Distribution of selected voxels and RSA patterns based on the real-time localizer data ($N = 27$). (a) Distribution of the real-time selected voxels. The color shade indicates how often each voxel was selected across participants. (b) Selection probability of each ROI (the top 10) across participants. The x-axis indicates the proportion of selected voxels in each region relative to the total number of selected voxels. (c) Group-level mean RDM and its 95% CIs, derived from the individual online analysis.

Int. J. Neur. Syst. 2026.36. Downloaded from www.worldscientific.com
by 84.118.51.191 on 05/04/26. Re-use and distribution is strictly not permitted, except for Open Access articles.

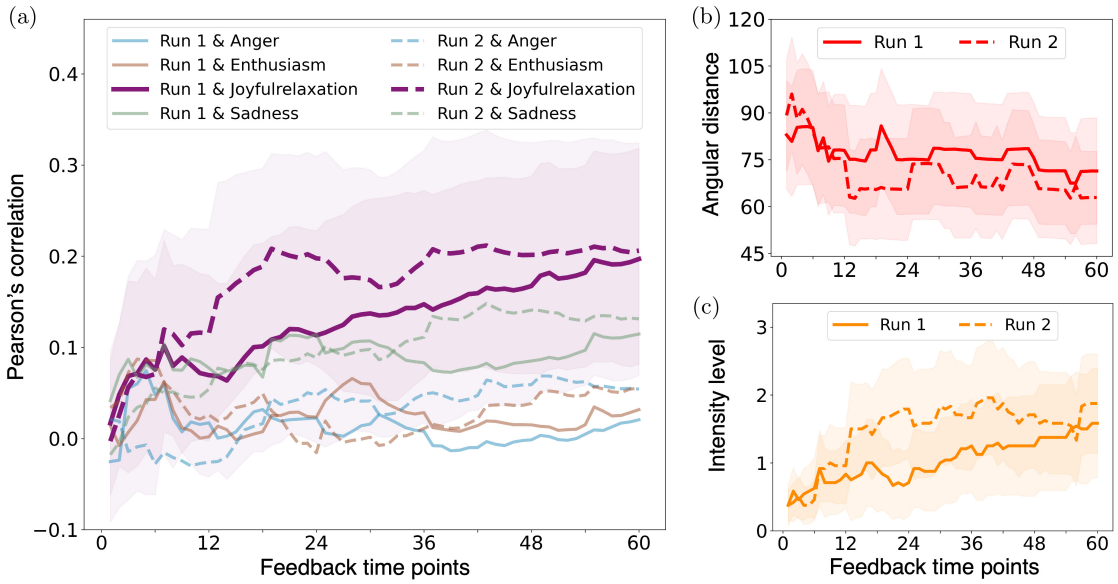

Fig. 4. Learning curves of neurofeedback performance metrics (target condition: joyful relaxation). The metrics include Pearson's correlation (a), angular distance (b), and intensity level (c). In each part, the mean value (across participants) and its 95% confidence interval are plotted over all feedback time points for two runs. Part A additionally shows, in the background, Pearson's correlations between the real-time brain pattern and each nontarget emotional base pattern.

base pattern for joyful relaxation became consistently higher than with the other emotional patterns after the first two blocks. This sustained advantage indicates that participants were able to reproducibly engage the target neural pattern, thereby maintaining effective modulation while differentiating it from other emotional states.

Additionally, as shown in Fig. 4(a), while correlations with the enthusiasm and anger patterns in the second run showed slight upward trends, all other nontarget emotional patterns remained stable over time. In contrast, correlations with the joyful relaxation pattern increased in both runs. The two derivative metrics also showed consistent improvement, reflected by decreasing angular distance (Fig. 4(b)) and increasing intensity level (Fig. 4(c)). The LMM analyses confirmed these trends as statistically significant (Table 1), with consistent effects across runs: positive slopes for Pearson's correlation (Run 1: $r = 0.002, p < 0.001$; Run 2: $r = 0.002, p < 0.001$) and intensity level (Run 1: $r = 0.017, p < 0.001$; Run 2: $r = 0.016, p < 0.001$), and negative slopes for angular distance (Run 1: $r = -0.172, p < 0.001$; Run 2: $r = -0.232, p < 0.001$). These results demonstrate a robust within-run learning effect, reflecting that participants were able to increasingly align their brain activity with the target pattern over time.

Figure 4 also revealed distinct patterns in learning dynamics between the two runs. For most time points, both Pearson's correlation and intensity level were higher in the second run than in the first, while angular distance was consistently lower after the first two blocks. LMM results demonstrated that initial performance in the second run was significantly better across all three metrics, but no significant differences in the linear slopes were observed between runs (Table 1). This pattern suggests that participants seem to begin the second run with an improved baseline regulation ability, likely reflecting carryover from the first run.

Visual inspection of the curves in Fig. 4 also suggested a shift in learning patterns: performance in the first run showed a steady progression, while improvements in the second run appeared to plateau after the early blocks. To formally account for these potential nonlinear trends, an exploratory model comparison using LRT indicated that including an additional quadratic time term provided a significantly better fit on all three metrics (Pearson's correlation: $\chi^2(2) = 14.25, p < 0.001$; angular

Int. J. Neur. Syst. 2026.36. Downloaded from www.worldscientific.com
by 84.118.51.191 on 05/04/26. Re-use and distribution is strictly not permitted, except for Open Access articles.

Int. J. Neur. Syst. 2026.36. Downloaded from www.worldscientific.com
by 84.118.51.191 on 05/04/26. Re-use and distribution is strictly not permitted, except for Open Access articles.

Table 1. Results of the LMM analysis for both runs (Formula: metric=time+Run+time:Run+(1|Participant)).

		Coef.	Std. Err.	z	p	95% CI
Pearson's correlation						
Intercept	Run1	0.061	0.050	1.236	0.217	(−0.036, 0.158)
	Run2	0.111	0.050	2.245	**0.025**	(0.014, 0.208)
	Run2 versus Run1	0.050	0.013	3.710	< **0.001**	(0.024, 0.076)
time	Run1	0.002	0.000	7.432	< **0.001**	(0.001, 0.003)
	Run2	0.002	0.000	6.431	< **0.001**	(0.001, 0.002)
	Run2 versus Run1	−0.001	0.000	−0.708	0.479	(−0.001, 0.001)
Angular distance						
Intercept	Run1	81.819	7.053	11.600	< **0.001**	(67.995, 95.643)
	Run2	77.177	7.053	10.942	< **0.001**	(63.353, 91.001)
	Run2 versus Run1	−4.642	2.240	−2.703	**0.038**	(−9.032, −0.252)
time	Run1	−0.172	0.044	−3.863	< **0.001**	(−0.259, −0.084)
	Run2	−0.232	0.044	−5.221	< **0.001**	(−0.319, −0.145)
	Run2 versus Run1	−0.060	0.063	−0.960	0.337	(−0.183, 0.063)
Intensity						
Intercept	Run1	0.525	0.293	1.794	0.073	(−0.049, 1.099)
	Run2	1.025	0.293	3.499	< **0.001**	(0.451, 1.599)
	Run2 versus Run1	0.499	0.084	5.921	< **0.001**	(0.334, 0.665)
time	Run1	0.017	0.002	9.995	< **0.001**	(0.013, 0.020)
	Run2	0.016	0.002	9.447	< **0.001**	(0.013, 0.019)
	Run2 versus Run1	−0.001	0.002	−0.388	0.698	(−0.006, 0.004)

distance: $\chi^2(2) = 7.10, p = 0.029$; intensity level: $\chi^2(2) = 70.12, p < 0.001$). The results from the exploratory quadratic model aligned with the observed patterns, revealing significant interactions between run and both the linear (time × run) and quadratic (time^2× run) terms across all three metrics (Table 2). For Pearson's correlation and intensity level, the interaction was characterized by a positive linear and negative quadratic term, indicating a sharper initial increase in the second run followed by a deceleration. For angular distance, the interaction showed a negative linear and positive quadratic term, reflecting a steeper initial decline that flattened over time. Overall, these results suggest a potential between-run learning effect, although the exploratory quadratic model adds greater complexity.

Initial versus final NF block comparison

Within each neurofeedback run, comparisons between the initial and final blocks revealed no significant changes in Pearson's correlation with the target base pattern (Run 1: $t_{(23)} = 1.811, p = 0.166$; Run 2: $t_{(23)} = 1.911, p = 0.137$; Fig. 5(a)) or in angular distance to the target condition (Run 1: $W = 119.0, p = 0.780$; Run 2: $W = 81.0, p = 0.098$; Fig. 5(b)). On the other hand, intensity level started near zero and ended significantly higher than the initial level (Run 1: $W = 10.5, p = 0.028$; Run 2: $W = 7.0, p = 0.005$; Fig. 5(c)). This initial-final within-run comparison indicated a trend toward improved performance from the beginning to the end of each run, though not all metrics reached statistical significance. The lack of significance in some metrics may be related to substantial inter-individual variability, as reflected by the relatively large SDs across participants in both runs (mean ± SD for initial versus final; Pearson's correlation: 0.06 ± 0.22 versus 0.18 ± 0.29 in Run 1, 0.05 ± 0.28 versus 0.19 ± 0.29 in Run 2; angular distance: 85.47 ± 45.40 versus 71.24 ± 42.33 in Run 1, 91.30 ± 44.46 versus 62.78 ± 37.14 in Run 2; intensity level: 0.48 ± 0.82 versus 1.50 ± 2.02 in Run 1; 0.42 ± 0.69 versus 1.85 ± 1.82 in Run 2; Fig. 5).

3.2.2. *Subjectively perceived control and neurofeedback performance*

At the end of each neurofeedback run, participants rated their perceived control over brain activity on a scale from 0 to 10 and reported the imagery strategies they had used, providing a subjective reference for their neurofeedback performance. Three sets of

Table 2. Results of the LMM analysis with quadratic time terms (Formula: metric=time+time^2+ Run+time:Run+time^2:Run+ (1|Participant)).

		Coef.	Std. Err.	z	p	95% CI
Pearson's correlation						
	Run1	0.060	0.051	1.175	0.240	(−0.040, 0.160)
Intercept	Run2	0.063	0.051	1.239	0.215	(−0.037, 0.164)
	Run2 versus Run1	0.003	0.022	0.145	0.885	(−0.041, 0.047)
	Run1	0.002	0.001	1.808	0.071	(−0.000, 0.004)
time	Run2	0.006	0.001	5.163	< **0.001**	(0.004, 0.008)
	Run2 versus Run1	0.004	0.002	2.372	**0.018**	(0.001, 0.007)
	Run1	−0.000	0.000	−0.088	0.930	(−0.000, 0.000)
$time^2$	Run2	−0.000	0.000	−3.775	< **0.001**	(−0.000, −0.000)
	Run2 versus Run1	−0.000	0.000	−2.607	**0.009**	(−0.000, −0.000)
Angular distance						
	Run1	81.099	7.362	11.016	< **0.001**	(66.671, 95.528)
Intercept	Run2	82.753	7.362	11.241	< **0.001**	(68.324, 97.182)
	Run2 versus Run1	1.654	3.730	0.443	0.657	(−5.656, 8.964)
	Run1	−0.108	0.192	−0.562	0.574	(−0.484, 0.268)
time	Run2	−0.725	0.192	−3.779	< **0.001**	(−1.101, −0.349)
	Run2 versus Run1	−0.617	0.271	−2.275	**0.023**	(−1.149, −0.085)
	Run1	−0.001	0.003	−0.341	0.733	(−0.007, 0.005)
$time^2$	Run2	0.008	0.003	2.643	**0.008**	(0.002, 0.014)
	Run2 versus Run1	0.009	0.004	2.110	**0.035**	(0.001, 0.017)
Intensity						
	Run1	0.583	0.303	1.922	0.055	(−0.011, 1.177)
Intercept	Run2	0.366	0.303	1.207	0.227	(−0.228, 0.960)
	Run2 versus Run1	−0.217	0.139	−1.562	0.118	(−0.489, 0.055)
	Run1	0.012	0.007	1.629	0.103	(−0.002, 0.026)
time	Run2	0.074	0.007	10.371	< **0.001**	(0.060, 0.088)
	Run2 versus Run1	0.062	0.010	6.182	< **0.001**	(0.043, 0.082)
	Run1	0.000	0.000	0.730	0.465	(−0.000, 0.000)
$time^2$	Run2	−0.001	0.000	−8.388	< **0.001**	(−0.001, −0.001)
	Run2 versus Run1	−0.001	0.000	−6.447	< **0.001**	(−0.001, −0.001)

ratings were missing, two of which were from participants who had completed both joyful relaxation runs.

Perceived control ratings demonstrated similar distributions across runs, with descriptive statistics (mean ± SD) of 4.64 ± 1.62 for the first run and 5.45 ± 2.28 for the second run. A paired t-test revealed no significant difference between runs ($t_{(21)} = 1.80, p = 0.086$), although there was a trend toward higher ratings in the second run. Our offline individual neurofeedback performance analyses showed that 22 out of 24 participants achieved successful regulation on at least one metric and 10 of them succeeded on all three metrics (see Table A.4), objectively reflecting their ability to control mental states.

Furthermore, as shown in Fig. 6, correlation analyses revealed a significant positive relationship between participants' perceived control ratings and their performance slopes for Pearson's correlation. In contrast, no significant relationships were observed for angular distance or intensity level. These findings were consistent across both neurofeedback runs, supporting the alignment between subjective reports and objective performance measures.

In addition, the MDS-based representational space was used to visualize descriptively each participant's modulation trajectory during neurofeedback runs (Fig. A.7). Although some trajectories diverged, most aligned with participants' perceived control ratings. Specifically, higher ratings were often accompanied by neurofeedback sequences that move progressively toward the corresponding base emotion as determined by the localizer. The distribution of emotion imagery strategies across participants is

Int. J. Neur. Syst. 2026.36. Downloaded from www.worldscientific.com
by 84.118.51.191 on 05/04/26. Re-use and distribution is strictly not permitted, except for Open Access articles.

Int. J. Neur. Syst. 2026.36. Downloaded from www.worldscientific.com
by 84.118.51.191 on 05/04/26. Re-use and distribution is strictly not permitted, except for Open Access articles.

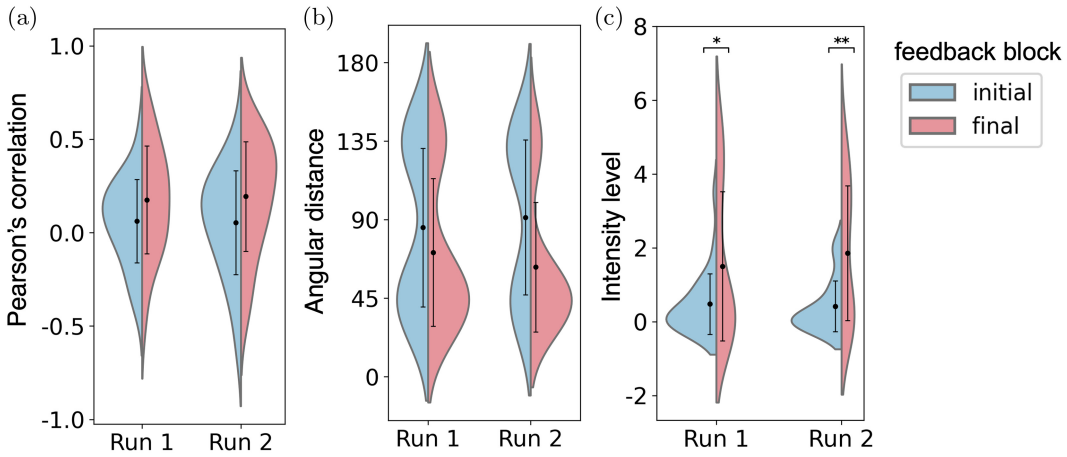

Fig. 5. (Color online) Comparison of neurofeedback performance metrics between initial and final feedback blocks (target condition: joyful relaxation). The median value of each metric within the corresponding block was compared. (a) Pearson's correlation coefficient between target pattern and the pattern extracted in the initial and final feedback blocks. (b) Angular distance in the initial and final feedback block, measured by calculating the angular distance between the red dot and the target stimulus on the CSM. (c) Same as (b) but using the thermometer reading of the target stimulus on the CSM as metric of intensity level. The violin plot shows the distribution of each metric across participants, and the error bar shows the corresponding mean and SD. Paired t-tests or Wilcoxon signed-rank tests were performed on the initial and final metrics. Results were considered significant (*: $p < 0.05$, **: $p < 0.01$) after Bonferroni correction ($n = 2$).

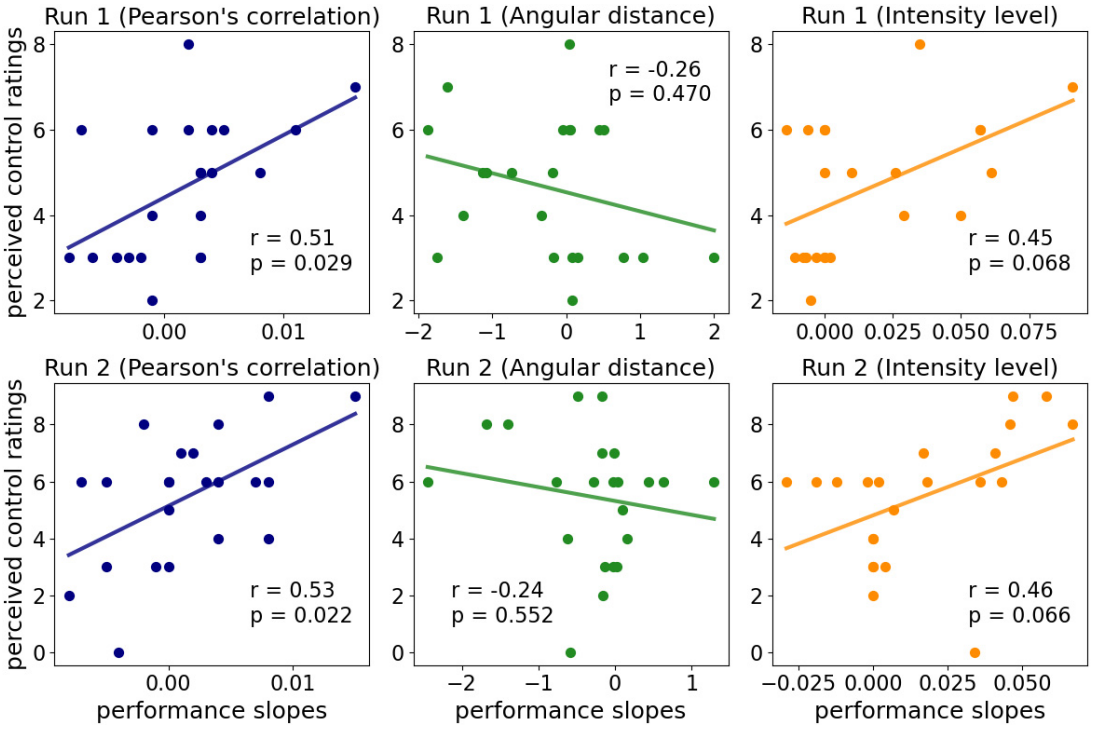

Fig. 6. Correlation analyses between participants' perceived control ratings and neurofeedback performance slopes for the condition joyful relaxation ($N = 22$). The perceived control ratings (y-axis) reflect participants' perceived control over brain activity, rated on a scale from 0 to 10. The performance slopes (x-axis) were obtained from individual linear regression models across the feedback time sequence. Statistical values were calculated using either Pearson's or Spearman's correlation, with Bonferroni correction across runs ($n = 2$) applied.

Int. J. Neur. Syst. 2026.36. Downloaded from www.worldscientific.com
by 84.118.51.191 on 05/04/26. Re-use and distribution is strictly not permitted, except for Open Access articles.

provided in Fig. A.6, with most participants relying on autobiographical recall to induce the target emotional states. Participants' post-run emotion ratings suggested successful engagement with the instructed emotional imagery. At the group level, subjective imagery ratings of the target emotion were moderate to high (mean ± SD for Run 1: 6.41 ± 1.40, Run 2: 6.95 ± 1.55), indicating that participants generally experienced the intended affective states during the task.

4. Discussion

This study investigated for the first time the feasibility of RSA-based rt-fMRI-sNF to navigate toward a predefined emotional state. To complement conventional univariate rt-fMRI-NF approaches, which primarily focus on signal amplitude, this work computed both the similarity and intensity of brain activity pattern using RSA as multivariate analysis method and delivered them to participants by a novel feedback visualization approach, the CSM. Our study provided four main insights: First, data from the localizer showed that RSA was able to differentiate between four different emotional states induced by mental imagery, providing for the first time proof-of-concept for the statistical sensitivity of RSA when used with the parameter choices made in our study. Second, participants were able to navigate their mental state toward a target state during consecutive neurofeedback training, providing evidence for the feasibility of our approach. Third, an analysis of participants' neurofeedback performance (based on the outcome metrics of correlation, similarity and intensity) from two neurofeedback runs suggested that self-regulation performance improved over time, indicating that participants learned to improve controlling the CSM-based visual feedback. Lastly, data showed that overall participants reported moderate control over the feedback, and this perceived control ratings were significantly correlated with the correlation metric, consistently across both neurofeedback runs.

Our pipeline included both univariate and multivariate processing steps, allowing us to compare results for both types of analyses and their performance in distinguishing between multiple affective states. In conventional univariate rt-fMRI-NF studies,[61,62] participants receive feedback based on the average activity within a predefined target region and learn to modulate this activity to influence the feedback intensity. While effective in simpler paradigms,[63,64] this approach becomes limited when applied to studies involving multiple emotional states,[65] as univariate methods have difficulty in capturing emotion-specific neural patterns, since different emotions often activate overlapping brain regions.[15,16] This limitation was also observed in our own data when performing univariate ROI analysis, such that the distributions of individual averaged contrast scores (task versus rest) showed substantial overlap and no significant differences across multiple emotional states for the selected emotion-related ROIs (see Fig. A.2). In contrast, multivariate methods analyze distributed multi-voxel brain activity patterns,[66,67] allowing for capturing the complex neural differences involved in processing multiple emotions. In our findings, the voxels contributing most to these patterns were primarily located in the dorsomedial and dorsolateral PFC (dmPFC, dlPFC), ACC, insula, and orbitofrontal cortex (OFC), which were found to be consistently implicated in emotion imagery in previous studies.[3] Furthermore, the group-level averaged RDM revealed clear distinctions between positive and negative emotional states. These findings show that our real-time RSA-based approach can reliably distinguish between multiple emotions, making it better suited than univariate methods for neurofeedback studies targeting complex emotional states.

Importantly, this work extended the rt-fMRI-sNF paradigm, previously tested using mental imagery of objects,[29,30] to the domain of emotion regulation. Object imagery involves the visualization of concrete external items (e.g. cats and chairs), relying on relatively objective and consistent visual-spatial representations.[68] In contrast, emotion imagery requires the mental simulation of internal emotional experiences, which are inherently subjective and influenced by personal context and memory.[69] The added cognitive and affective complexity makes emotion

Int. J. Neur. Syst. 2026.36. Downloaded from www.worldscientific.com
by 84.118.51.191 on 05/04/26. Re-use and distribution is strictly not permitted, except for Open Access articles.

imagery more challenging to engage and regulate. Our group-level offline assessment of neurofeedback performance supports the feasibility of applying this paradigm to emotion regulation. Specifically, the results showed a reduced angular distance between the real-time activity pattern and the target emotion pattern, as well as increased activation intensity in the final emotion imagery block compared to the first. Besides, within-run learning trends showed significant and consistent improvement across three evaluation metrics. These results suggest that participants were able to progressively align their brain activity with the target emotional states, demonstrating effective engagement with visual feedback. Moreover, higher initial performance (from linear model) and larger learning rate (from exploratory quadratic model) in the second neurofeedback run were observed. This suggests that participants may have retained effective strategies from the first run, enabling more efficient engagement during the subsequent run.

In addition, this work examined the effectiveness of the CSM-based visual feedback, a novel feedback presentation method, in the context of emotion regulation training. Conventional univariate rt-fMRI-NF paradigms typically use a thermometer-like display to reflect brain activation intensity. The previous rt-fMRI-sNF paradigm for object imagery[30,29] focused on pattern similarity by projecting the real-time and target activity patterns into a two-dimensional space according to the pairwise dissimilarities. Building on this approach and its variant,[31] the CSM placed multiple thermometers and a moving red dot in a circular arrangement, providing feedback on both pattern similarity and activation intensity. Our individual neurofeedback performance results indicated successful learning trends in most participants (see Table A.4). Of the 24 participants, 22 achieved successful regulations in at least one metric during one or more neurofeedback runs, and 10 participants succeeded across all three metrics during at least one neurofeedback run. These findings suggest that participants were able to engage with and benefit from the feedback, supporting the practical usability of the CSM-based visual feedback for individual-level emotion regulation. This notion is further supported by the relationship between participants' subjective perceptions and their objectively measured ability to regulate brain activity through neurofeedback. Participants generally reported moderate perceived control, suggesting a consistent subjective experience during the experiment. While perceived control ratings showed no significant difference between runs, exploratory descriptive analyses using MDS indicated that for most participants with moderate to high control ratings (> 6), the similarity between neurofeedback and base patterns increased over time (see Fig. A.7). Importantly, a significant positive association between perceived control ratings and neurofeedback performance on the Pearson's correlation metric was observed. This alignment between subjective perception and objectively calculated performance further underscores the feasibility of the rt-fMRI-sNF paradigm, indicating that participants can meaningfully interpret and utilize feedback to modulate neural activity.

Furthermore, this work investigated group-level activation patterns during the localizer and neurofeedback runs (see Fig. A.1). The localizer task, focusing on emotion generation, primarily engaged the prefrontal regions, including the dlPFC, dmPFC and OFC. On the other hand, the neurofeedback runs, emphasizing emotion regulation, showed descriptively stronger activation in the insula and ventromedial PFC (vmPFC). These descriptive differences align with prior research on the neural correlates of emotion generation and regulation. Specifically, the vmPFC is extensively involved in modulating affective responses and integrating feedback to guide emotional adjustments.[70] The insula, especially its anterior portion, plays a key role in interoceptive awareness, enabling individuals to monitor and regulate internal emotional states based on real-time feedback.[71]

5. Limitations

While the present findings highlight the potential advantages of a multivariate neurofeedback approach in the context of emotion regulation, several limitations should be considered and addressed in future work.

Int. J. Neur. Syst. 2026.36. Downloaded from www.worldscientific.com
by 84.118.51.191 on 05/04/26. Re-use and distribution is strictly not permitted, except for Open Access articles.

One key limitation of this study is the insufficient data for neurofeedback performance comparisons across emotions. While 24 participants completed repeated neurofeedback runs for the emotion of joyful relaxation, only 14 participants performed a single run for sadness. This imbalance reduced statistical power and precluded systematic within- and between-run comparisons across emotions. The rt-fMRI-sNF paradigm requires multiple functional localizer runs to generate base patterns prior to neurofeedback training, which limits the number of neurofeedback runs that can be performed within a single session. Besides, a long measurement may lead to participant fatigue and reduce the mental imagery quality in emotion-based studies. For instance, when participants become tired or uncomfortable, it may be particularly challenging for them to generate and regulate high-arousal positive emotions effectively. A potential solution to this constraint is adopting a multi-session design, in which localizer and neurofeedback runs are performed on separate days to allow for more extensive training and data collection. Depending on the study design, such an approach would likely require precise alignment of functional localizer data across measurement sessions to ensure comparability.[72,73] Moreover, multi-session neurofeedback training protocols will have to deal with potential challenges related to the test–retest reliability of emotion processing[74,75] and, in particular, emotional mental imagery. However, a multivariate approach likely also entails an improvement in relation to this challenge compared to multi-session univariate emotion regulation neurofeedback paradigms.[76]

As a hardware-related limitation, a voxel size of $3\,\mathrm{mm}^3$ at 3 Tesla combined with spatial smoothing of the functional data (6 mm Gaussian kernel) was used in this study. The resulting effective resolution might not optimally support differentiating overlapping patterns of different emotions. It remains to be seen whether the increased signal to noise and/or higher spatial resolution of 7 Tesla ultra-high field fMRI will result in substantial improvements in rt-RSA neurofeedback. While not as widespread as 3 Tesla scanners, clinical 7 Tesla devices are becoming increasingly available, which could be relevant for future clinical applications of semantic neurofeedback of emotions.

In addition, between-subject variability in emotional mental imagery and its influence on neurofeedback performance warrant further investigation. To provide a personalized training approach, our employed real-time RSA-based method selected individualized target voxels and generated participant-specific RDMs. However, varying output RDMs (Fig. 3(c)) across participants were observed during the localizer, which may have introduced differences in regulation difficulty among participants. Incorporating a screening step to assess baseline mental imagery capabilities, along with enhanced pre-experimental training, may help reduce the effects of individual differences and yield improved neurofeedback performance.

Lastly, as a feasibility study, this work has several limitations that should be considered when interpreting the findings and that inform directions for future research. First, no *a priori* power analysis was conducted to determine a target sample size, as the primary aim was to assess the technical and conceptual viability of the rt-fMRI-sNF paradigm rather than to establish effect sizes or test clinical or behavioral symptom change. Second, the representational model was intentionally simplified, focusing primarily on valence-related distinctions between emotional states; future studies could benefit from incorporating more complex model RDMs that capture additional affective dimensions, such as arousal. In addition, several hyperparameters, including voxel selection thresholds, were determined heuristically based on pilot data to ensure stable real-time performance. While suitable for feasibility testing, these choices would benefit from systematic optimization in larger samples, which may result in better neurofeedback performance. The absence of control or sham neurofeedback conditions further limits causal inference and generalizability, underscoring the need for controlled designs in subsequent studies. Finally, this work did not aim to compare RSA-based neurofeedback with alternative multivariate approaches such as classifier-based methods[77]; such comparisons represent an important avenue for future research to better characterize the relative advantages of different multivariate neurofeedback frameworks.

Int. J. Neur. Syst. 2026.36. Downloaded from www.worldscientific.com
by 84.118.51.191 on 05/04/26. Re-use and distribution is strictly not permitted, except for Open Access articles.

6. Conclusion

This study explored the feasibility of an rt-fMRI-sNF paradigm for guiding emotion regulation. By incorporating an RSA-informed CSM to visualize both the similarity and intensity of brain activity in real time, participants were able to navigate among distinct emotional states using mental imagery. Our localizer findings showed the effectiveness of RSA in differentiating overlapping emotional representations, highlighting its potential to capture the complexity of affective brain patterns. Group-level analyses revealed performance improvements within each neurofeedback run and higher initial performance in the second run, suggesting that participants can effectively modulate and maintain target emotional states when guided by RSA-informed feedback. At the individual level, most participants achieved successful regulation on at least one performance metric, and their perceived control ratings were positively associated with objective neurofeedback outcomes. Overall, this paradigm offers a promising multivariate framework for investigating and training emotion regulation through neurofeedback.

Acknowledgments

This research was funded by the RWTH Aachen University Exploratory Research Space (ERS) OPEN Seed Fund (OPFS727), the START Program of the Faculty of Medicine the grant number (019/23), RWTH Aachen, and the Junior Principal Investigator (JPI) fellowship funded by the Excellence Strategy of the Federal Government and the Laender (Grant No. JPI074-21). Xuelei Wang was funded by the China Scholarship Council (No. 202206060018). The study was also supported by the Brain Imaging Facility of the Interdisciplinary Center for Clinical Research (IZKF) within the Faculty of Medicine at RWTH Aachen University. David M. A. Mehler and Jana Zweerings contributed equally to this work.

Data Availability Statement

The data supporting the findings of this study will be made publicly available in a suitable repository at a later date.

AI Usage Statement

During the preparation of this work the author(s) used ChatGPT in order to assist with language refinement. After using this tool/service, the author(s) reviewed and edited the content as needed and take (s) full responsibility for the content of the published paper.

Conflicts of Interest

The authors declare no conflicts of interest.

Appendix A

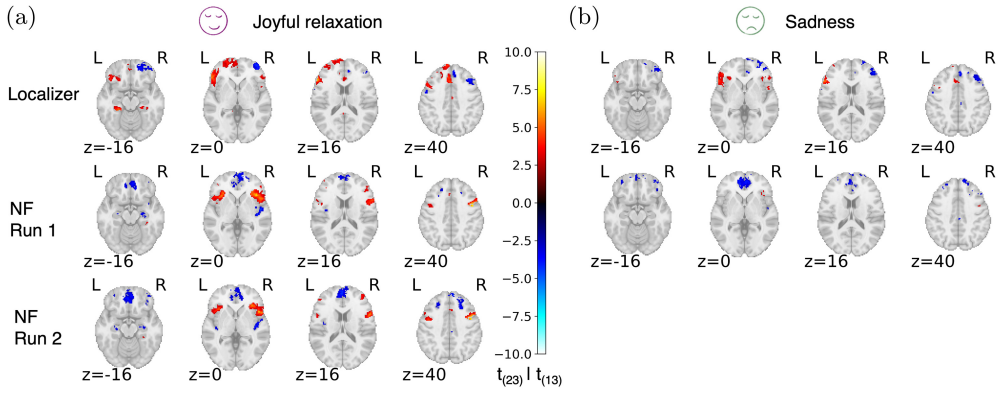

Fig. A.1. Group-level univariate analysis for NF runs and corresponding localizer runs targeting the same emotion. For consistency, univariate patterns for localizer runs were reconstructed using the same participant groups as in the respective NF runs. (a) Joyful relaxation ($N = 24$). (b) Sadness ($N = 14$).

Int. J. Neur. Syst. 2026.36. Downloaded from www.worldscientific.com
by 84.118.51.191 on 05/04/26. Re-use and distribution is strictly not permitted, except for Open Access articles.

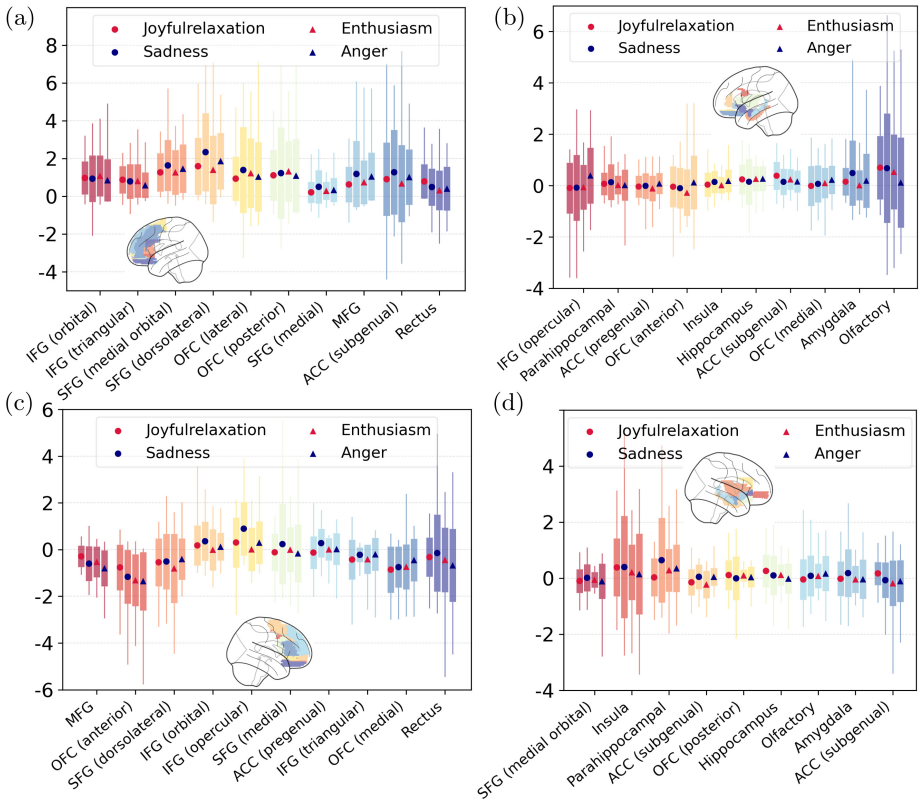

Fig. A.2. ROI analysis results across all 39 regions, based on the average activity of all voxels within each ROI. Regions are ordered by group-level activity across conditions for each hemisphere. (a) Top 10 regions in the left hemisphere. (b) Bottom 10 regions in the left hemisphere. (c) Top 10 regions in the right hemisphere. (d) Bottom 9 regions in the right hemisphere.

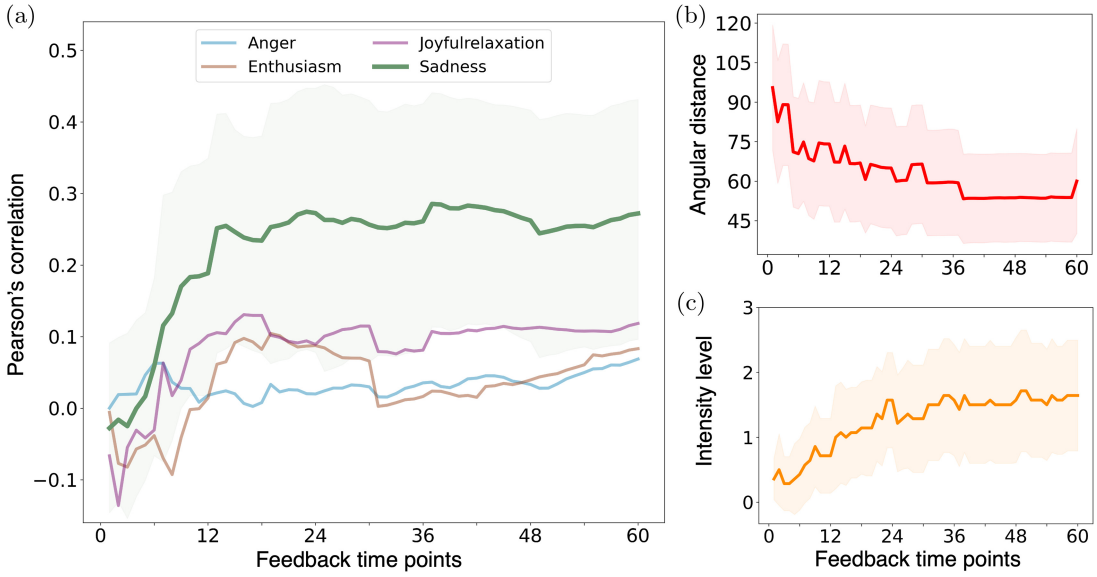

Fig. A.3. Learning curves of neurofeedback performance metrics (target condition: sadness). The metrics include Pearson's correlation (a), angular distance (b), and intensity level (c). In each part, the mean value (across participants) and its 95% confidence interval are plotted over all feedback time points for two runs. Part A additionally shows, in the background, Pearson's correlations between the real-time brain pattern and each nontarget emotional base pattern.

Int. J. Neur. Syst. 2026.36. Downloaded from www.worldscientific.com
by 84.118.51.191 on 05/04/26. Re-use and distribution is strictly not permitted, except for Open Access articles.

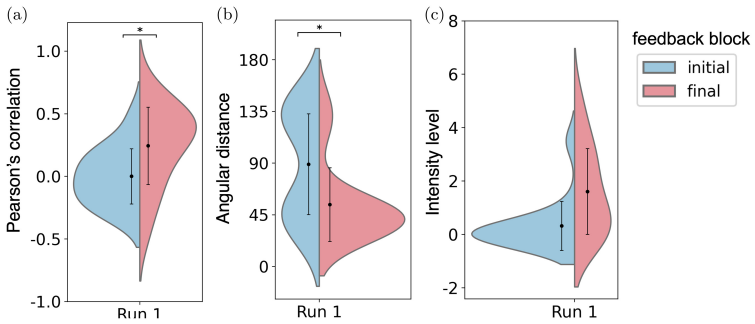

Fig. A.4. (Color online) Comparison of neurofeedback performance metrics between initial and final feedback blocks (target condition: sadness). The median value of each metric within the corresponding block was extracted and compared. (a) Pearson's correlation coefficient between target pattern and the pattern extracted in the first and last feedback blocks. (b) Angular distance in the first and last feedback block, measured by calculating the angular distance between the red dot and the target stimulus on the CSM. (c) Same as (b) but using the thermometer reading of the target stimulus on the CSM as metric of intensity level. The violin plot shows the distribution of each metric across participants, and the error bar shows the corresponding mean and SD. Paired t-tests or Wilcoxon signed-rank tests were performed on the initial and final metrics. Results were considered significant (*: $p < 0.05$, **: $p < 0.01$) after Bonferroni correction ($n = 2$).

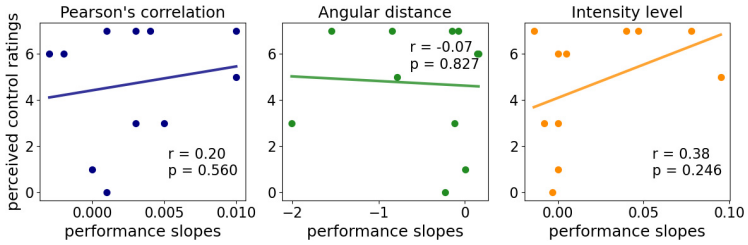

Fig. A.5. Correlation analyses between participants' perceived control ratings and neurofeedback performance slopes for sadness ($N = 11$). The perceived control ratings (y-axis) reflect participants' perceived control over brain activity, rated on a scale from 0 to 10. The performance slopes (x-axis) were obtained from individual linear regression models across the feedback time sequence. Statistical values were calculated using either Pearson's or Spearman's correlation (not corrected).

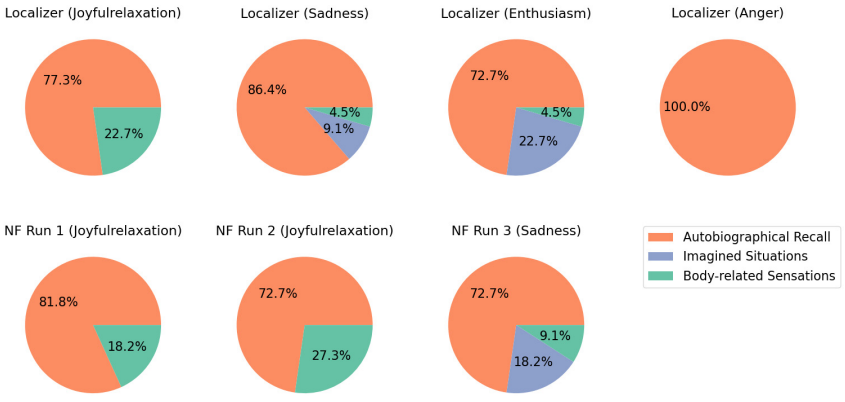

Fig. A.6. Distribution of emotion imagery strategies across participants. Questionnaires were collected for all localizer runs and the first two NF runs ($N = 22$), and for the final NF run ($N = 11$). Emotion imagination strategies were grouped into three categories: (1) Autobiographical recall — drawing on personal experiences (e.g. remembering a family gathering for joyful relaxation, or recalling a breakup to induce sadness); (2) Imagined situations — constructing hypothetical or unreal scenarios (e.g. picturing oneself winning a competition for enthusiasm, or being treated unfairly to elicit anger); and (3) Body-related sensations — focusing on physical feelings associated with emotions (e.g. a light and relaxed body state for joyful relaxation, or rising heat for anger).

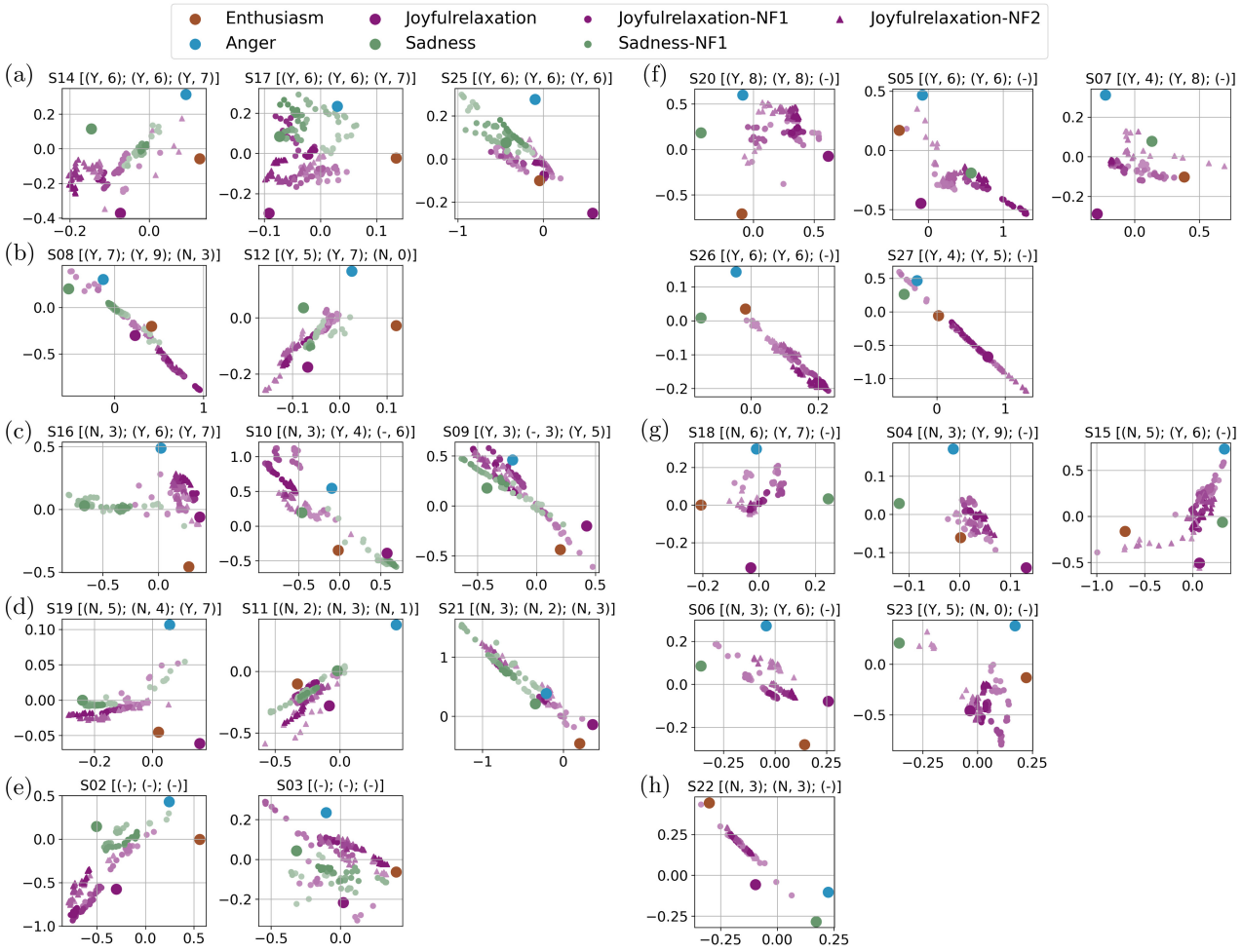

Fig. A.7. (Color online) Individual modulation trajectories during neurofeedback runs visualized with MDS (the left part from a to e is for participants with both joyful relaxation and sadness runs, $N = 13$; the right part from f to h is for participants with only two joyful relaxation runs, $N = 11$). The X and Y axes represent the two scaled dimensions from MDS. For each participant, the four localizer base patterns were reduced to two dimensions using MDS and plotted as anchor points (larger circles) with colors indicating the corresponding localizer emotion. Neurofeedback data were then projected into the same representational space for joyful relaxation (smaller circles for run 1 and smaller triangles for run 2) and for sadness (smaller circle) in the corresponding color, The shade of the markers indicates time progression, with darker shades showing later time points. Subfigure titles show the participant number and their perceived control ratings (Y/N=yes/no), followed by the reported rating score ('—' denotes no ratings collected or no corresponding run). Subpanels are arranged in descending order according to the number of positive ratings.

Int. J. Neur. Syst. 2026.36. Downloaded from www.worldscientific.com
by 84.118.51.191 on 05/04/26. Re-use and distribution is strictly not permitted, except for Open Access articles.

Table A.1. Predefined emotion-related regions. Subcortical regions, including amygdala and hippocampus, are based on the Harvard-Oxford atlas (maximum probability maps, thresholded at 25%, 1 mm resolution). Cortical regions are based on the Schaefer atlas (17-network parcellation, 200 parcels, 1 mm resolution). The coordinates shown '—' indicate that the corresponding labels were not defined in that hemisphere.

			MNI coordinates	
Label	Network	Region	left	right
Amygdala	—	amygdala	(−23, −5, −18)	(23, −4, −18)
Hippocampus	—	hippocampus	(−25, −22, −14)	(26, −21, −14)
ContA_Cingm_1	control A	middle cingulate cortex	(−3, 4, 30)	(5, 3, 30)
ContA_PFCd_1	control A	dorsal prefrontal cortex	(−22, 6, 62)	(26, 7, 58)
ContA_PFCl_1	control A	lateral prefrontal cortex	(−44, 20, 27)	(52, 11, 21)
ContA_PFCl_2	control A	lateral prefrontal cortex	(−48, 6, 29)	(46, 24, 26)
ContA_PFCl_3	control A	lateral prefrontal cortex	(−43, 6, 43)	—
ContA_PFClv_1	control A	lateral ventral prefrontal cortex	(−42, 40, 16)	—
ContB_PFCld_1	control B	lateral dorsal prefrontal cortex	—	(41, 33, 37)
ContB_PFCld_2	control B	lateral dorsal prefrontal cortex	—	(42, 14, 49)
ContB_PFCld_3	control B	lateral dorsal prefrontal cortex	—	(23, 24, 53)
ContB_PFCl_1	control B	lateral prefrontal cortex	(−40, 19, 49)	—
ContB_PFClv_1	control B	lateral ventral prefrontal cortex	(−42, 49, −6)	(36, 46, −13)
ContB_PFClv_2	control B	lateral ventral prefrontal cortex	(−28, 58, 8)	(29, 58, 5)
ContB_PFCmp_1	control B	medial posterior prefrontal cortex	—	(7, 25, 55)
ContC_Cingp_1	control C	posterior cingulate cortex	(−5, −29, 28)	(5, −24, 31)
DefaultA_PFCd_1	default A	dorsal prefrontal cortex	(−24, 25, 49)	(29, 30, 42)
DefaultA_PFCm_1	default A	medial prefrontal cortex	(−6, 36, −10)	(8, 42, 4)
DefaultA_PFCm_2	default A	medial prefrontal cortex	(−12, 63, −6)	(6, 29, 15)
DefaultA_PFCm_3	default A	medial prefrontal cortex	(−6, 44, 7)	(8, 58, 18)
DefaultB_PFCd_1	default B	dorsal prefrontal cortex	(−8, 59, 21)	(15, 46, 44)
DefaultB_PFCd_2	default B	dorsal prefrontal cortex	(−11, 47, 45)	—
DefaultB_PFCd_3	default B	dorsal prefrontal cortex	(−3, 33, 43)	—
DefaultB_PFCd_4	default B	dorsal prefrontal cortex	(−9, 17, 63)	—
DefaultB_PFCv_1	default B	ventral prefrontal cortex	(−35, 20, −13)	(51, 28, 0)
DefaultB_PFCv_2	default B	ventral prefrontal cortex	(−32, 42, −13)	—
DefaultB_PFCv_3	default B	ventral prefrontal cortex	(−46, 31, −7)	—
DefaultB_PFCv_4	default B	ventral prefrontal cortex	(−52, 22, 8)	—
DefaultC_PHC_1	default C	parahippocampal cortex	(−26, −32, −18)	(28, −36, −14)
LimbicB_OFC_1	limbic B	orbital frontal cortex	(−24, 22, −20)	(12, 39, −22)
LimbicB_OFC_2	limbic B	orbital frontal cortex	(−10, 35, −21)	(28, 22, −19)
LimbicB_OFC_3	limbic B	orbital frontal cortex	—	(5, 37, −14)
LimbicB_OFC_4	limbic B	orbital frontal cortex	—	(15, 64, −8)
SalVentAttnA_FrOper_1	salience/ ventral attention A	frontal operculum	(−39, 1, 11)	(43, 7, 4)
SalVentAttnA_FrOper_2	salience/ ventral attention A	frontal operculum	(−51, 9, 11)	—
SalVentAttnA_Ins_1	salience/ ventral attention A	insula	(−39, −4, −4)	(41, 6, −15)
SalVentAttnA_Ins_2	salience/ ventral attention A	insula	—	(46, −4, −4)
SalVentAttnB_Ins_1	salience/ ventral attention B	insula	(−33, 20, 5)	(34, 21, −8)

Int. J. Neur. Syst. 2026.36. Downloaded from www.worldscientific.com
by 84.118.51.191 on 05/04/26. Re-use and distribution is strictly not permitted, except for Open Access articles.

Table A.1. (*Continued*)

Label	Network	Region	MNI coordinates left	MNI coordinates right
SalVentAttnB_Ins_2	salience/ ventral attention B	insula	—	(36, 24, 5)
SalVentAttnB_PFCl_1	salience/ ventral attention B	lateral prefrontal cortex	(−28, 43, 31)	(30, 48, 27)
SalVentAttnB_PFClv_1	salience/ ventral attention B	lateral ventral prefrontal cortex	—	(43, 45, 10)
SalVentAttnB_PFCmp_1	salience/ ventral attention B	medial posterior prefrontal cortex	(−6, 30, 25)	(7, 31, 28)

Table A.2. Regions used for offline analysis (more than 50% overlapped with the predefined regions, based on AAL3 atlas). AAL=automatic anatomical labeling.

Anatomical description	AAL3 label	Overlap/%	AAL3 label	Overlap/%
Superior frontal gyrus, dorsolateral	Frontal_Sup_2_L	70.76	Frontal_Sup_2_R	65.00
Middle frontal gyrus	Frontal_Mid_2_L	74.42	Frontal_Mid_2_R	74.88
Inferior frontal gyrus, opercular part	Frontal_Inf_Oper_L	79.38	Frontal_Inf_Oper_R	78.34
Inferior frontal gyrus, triangular part	Frontal_Inf_Tri_L	81.02	Frontal_Inf_Tri_R	68.99
Inferior frontal gyrus pars orbitalis	Frontal_Inf_Orb_2_L	83.91	Frontal_Inf_Orb_2_R	69.68
Olfactory cortex	Olfactory_L	71.48	Olfactory_R	77.78
Superior frontal gyrus, medial	Frontal_Sup_Medial_L	72.03	Frontal_Sup_Medial_R	78.12
Superior frontal gyrus, medial orbital	Frontal_Med_Orb_L	83.87	Frontal_Med_Orb_R	89.14
Gyrus rectus	Rectus_L	84.04	Rectus_R	88.72
Medial orbital gyrus	OFCmed_L	73.27	OFCmed_R	66.02
Anterior orbital gyrus	OFCant_L	73.36	OFCant_R	65.59
Posterior orbital gyrus	OFCpost_L	67.90	OFCpost_R	57.40
Lateral orbital gyrus	OFClat_L	85.28	—	—
Insula	Insula_L	77.56	Insula_R	81.30
Hippocampus	Hippocampus_L	72.32	Hippocampus_R	76.00
Parahippocampal gyrus	ParaHippocampal_L	55.62	ParaHippocampal_R	50.35
Amygdala	Amygdala_L	87.27	Amygdala_R	77.02
Anterior cingulate cortex, subgenual	ACC_sub_L	94.64	ACC_sub_R	97.73
Anterior cingulate cortex, pregenual	ACC_pre_L	96.17	ACC_pre_R	92.90
Anterior cingulate cortex, supracallosal	ACC_sup_L	88.43	ACC_sup_R	90.81

Int. J. Neur. Syst. 2026.36. Downloaded from www.worldscientific.com
by 84.118.51.191 on 05/04/26. Re-use and distribution is strictly not permitted, except for Open Access articles.

Table A.3. Individual feedback performance for sadness ($N = 14$), assessed using linear regression across time (excluding the first two time points). The "success" column indicates whether the corresponding metric showed a significant improvement ($p < 0.05$, FDR-corrected). Specifically, success was defined as a significantly positive slope for Pearson's correlation and intensity level, and a significantly negative slope for angular distance.

		Pearson's correlation			Angular distance			Intensity level		
Sub_id	Run	Slope	p-value	Success	Slope	p-value	Success	Slope	p-value	Success
S01	Run 1	0.001	0.39	N	−0.212	< 0.001	Y	0.06	< 0.001	Y
S02	Run 1	0.001	0.232	N	0.015	0.602	N	−0.02	0.013	N
S03	Run 1	0.002	0.002	Y	−0.624	0.089	N	0	1	N
S08	Run 1	0.005	< 0.001	Y	−2.008	< 0.001	Y	0	1	N
S09	Run 1	0.01	< 0.001	Y	−0.783	< 0.001	Y	0.095	< 0.001	Y
S10	Run 1	−0.003	< 0.001	N	0.147	0.251	N	0	1	N
S11	Run 1	0	0.667	N	0.01	0.602	N	0	1	N
S12	Run 1	0.001	0.139	N	−0.23	0.089	N	−0.003	0.069	N
S14	Run 1	0.001	0.121	N	−0.073	< 0.001	Y	0.078	< 0.001	Y
S16	Run 1	0.004	0.013	Y	−0.15	0.342	N	−0.014	0.013	N
S17	Run 1	0.01	< 0.001	Y	−1.547	< 0.001	Y	0.04	< 0.001	Y
S19	Run 1	0.003	< 0.001	Y	−0.843	< 0.001	Y	0.047	< 0.001	Y
S21	Run 1	0.003	0.007	Y	−0.116	0.001	Y	−0.008	0.451	N
S25	Run 1	−0.002	0.015	N	0.159	< 0.001	N	0.005	0.291	N

Table A.4. Individual feedback performance for joyful relaxation ($N = 24$), assessed using linear regression across time (excluding the first two time points). The "success" column indicates whether the corresponding metric showed a significant improvement ($p < 0.05$, FDR-corrected). Specifically, success was defined as a significantly positive slope for Pearson's correlation and intensity level, and a significantly negative slope for angular distance.

		Pearson's correlation			Angular distance			Intensity level		
Sub_id	Run	Slope	p-value	Success	Slope	p-value	Success	Slope	p-value	Success
S02	Run 1	0.012	< 0.001	Y	−0.532	< 0.001	Y	0.067	< 0.001	Y
	Run 2	0	0.821	N	0.07	< 0.001	N	0.02	0.005	Y
S03	Run 1	0	0.779	N	1.502	< 0.001	N	−0.031	< 0.001	N
	Run 2	0.008	< 0.001	Y	0.636	0.001	N	0	1	N
S04	Run 1	−0.002	0.035	N	1.035	0.006	N	0.002	1	N
	Run 2	0.015	< 0.001	Y	−0.48	0.023	Y	0.058	< 0.001	Y
S05	Run 1	−0.007	< 0.001	N	0.509	< 0.001	N	−0.006	0.008	N
	Run 2	0.004	< 0.001	Y	0.636	0.027	N	−0.019	< 0.001	N
S06	Run 1	0.003	< 0.001	Y	−1.749	< 0.001	Y	0	1	N
	Run 2	−0.005	< 0.001	N	−2.445	< 0.001	Y	0.043	< 0.001	Y
S07	Run 1	−0.001	0.382	N	−0.338	< 0.001	Y	0.029	< 0.001	Y
	Run 2	−0.002	0.004	N	−1.4	< 0.001	Y	0.046	< 0.001	Y
S08	Run 1	0.016	< 0.001	Y	−1.614	< 0.001	Y	0.091	< 0.001	Y
	Run 2	0.008	< 0.001	Y	−0.171	< 0.001	Y	0.047	< 0.001	Y
S09	Run 1	−0.006	< 0.001	N	2.002	< 0.001	N	−0.008	0.04	N
	Run 2	−0.001	0.149	N	−0.138	< 0.001	Y	0	1	N
S10	Run 1	−0.003	< 0.001	N	−0.167	< 0.001	Y	0	1	N
	Run 2	0.004	< 0.001	Y	0.155	< 0.001	N	0	1	N
S11	Run 1	−0.001	0.357	N	0.087	< 0.001	N	−0.005	0.008	N
	Run 2	0	0.969	N	0.027	0.123	N	0.004	0.716	N
S12	Run 1	0.008	< 0.001	Y	−1.077	< 0.001	Y	0.026	< 0.001	Y
	Run 2	0.001	0.121	N	−0.016	0.143	N	0.041	< 0.001	Y
S14	Run 1	0.005	< 0.001	Y	0.048	0.022	N	0.057	< 0.001	Y

Int. J. Neur. Syst. 2026.36. Downloaded from www.worldscientific.com
by 84.118.51.191 on 05/04/26. Re-use and distribution is strictly not permitted, except for Open Access articles.

Table A.4. (*Continued*)

		Pearson's correlation			Angular distance			Intensity level		
Sub_id	Run	Slope	p-value	Success	Slope	p-value	Success	Slope	p-value	Success
	Run 2	0.003	< 0.001	Y	−0.282	0.023	Y	0.018	0.004	Y
S15	Run 1	0.004	< 0.001	Y	−1.136	< 0.001	Y	0.01	< 0.001	Y
	Run 2	0	0.99	N	0.444	0.228	N	−0.002	0.853	N
S16	Run 1	0.003	< 0.001	Y	0.781	< 0.001	N	−0.011	0.002	N
	Run 2	0	0.432	N	1.293	< 0.001	N	−0.012	0.013	N
S17	Run 1	0.002	< 0.001	Y	0.442	0.012	N	−0.014	0.291	N
	Run 2	0.008	< 0.001	Y	0.034	0.074	N	0.002	1	N
S18	Run 1	0.004	< 0.001	Y	0.056	0.003	N	0	1	N
	Run 2	0.002	< 0.001	Y	−0.17	0.606	N	0.017	< 0.001	Y
S19	Run 1	0.003	0.077	N	−0.741	< 0.001	Y	0	1	N
	Run 2	0.008	< 0.001	Y	−0.619	0.003	Y	0	1	N
S20	Run 1	0.002	< 0.001	Y	0.04	0.275	N	0.035	0.024	Y
	Run 2	0.004	< 0.001	Y	−1.68	< 0.001	Y	0.067	< 0.001	Y
S21	Run 1	−0.004	0.015	N	0.153	0.137	N	−0.003	0.224	N
	Run 2	−0.008	< 0.001	N	−0.163	< 0.001	Y	0	1	N
S22	Run 1	−0.008	< 0.001	N	0.076	< 0.001	N	−0.007	0.037	N
	Run 2	−0.005	< 0.001	N	−0.018	0.219	N	0	1	N
S23	Run 1	0.003	< 0.001	Y	−0.186	< 0.001	Y	0.061	< 0.001	Y
	Run 2	−0.004	0.001	N	−0.586	0.001	Y	0.034	< 0.001	Y
S25	Run 1	−0.001	0.117	N	−1.875	< 0.001	Y	0	1	N
	Run 2	−0.007	< 0.001	N	−0.762	< 0.001	Y	−0.029	0.034	N
S26	Run 1	0.011	< 0.001	Y	−0.04	0.131	N	0.057	< 0.001	Y
	Run 2	0.007	< 0.001	Y	−0.023	0.101	N	0.036	< 0.001	Y
S27	Run 1	0.003	0.01	Y	−1.392	< 0.001	Y	0.05	< 0.001	Y
	Run 2	0	0.99	N	0.097	0.009	N	0.007	0.621	N

Int. J. Neur. Syst. 2026.36. Downloaded from www.worldscientific.com
by 84.118.51.191 on 05/04/26. Re-use and distribution is strictly not permitted, except for Open Access articles.

Int. J. Neur. Syst. 2026.36. Downloaded from www.worldscientific.com
by 84.118.51.191 on 05/04/26. Re-use and distribution is strictly not permitted, except for Open Access articles.

Appendix B

CRED-nf checklist summary

22 September, 2025

Manuscript title: Toward navigating emotional states using real-time representational similarity analysis fMRI neurofeedback - a feasibility study
Corresponding Author: David M. A. Mehler; Jana Zweerings
Corresponding author email: dmehler@ukaachen.de; jzweerings@ukaachen.de

Item No.	Checklist item	Manuscript Details
Pre-experiment		
1a	Pre-register experimental protocol and planned analyses	This feasibility study was preregistered (https://osf.io/5ybuw).
1b	Justify sample size	Because this work was designed as a feasibility study, no formal a priori power analysis was conducted; instead, sample size was determined based on practical constraints and the goal of evaluating methodological feasibility.
Control groups		
2a	Employ control group(s) or control condition(s)	*This experiment did not include a control group or control condition*
2b	When leveraging experimental designs where a double-blind is possible, use a double-blind	*NA: A double-blind was not appropriate for this experiment*
2c	Blind those who rate the outcomes	*NA: There was only one participant group*
	Blind those who analyse the data	*NA: There was only one participant group*
2d	Examine to what extent participants and experimenters remain blinded	*NA: There was only one participant group*
2e	In clinical efficacy studies, employ a standard-of-care intervention group as a benchmark for improvement	*NA: This is not a clinical efficacy study*
Control measures		
3a	Collect data on psychosocial factors	Prior to and after the measurement, all participants completed questionnaires assessing their current mood state and their ability to regulate emotions, as measured by the Profile Of Mood States (POMS) (McNair, 1971) and Emotion Regulation Questionnaire (ERQ) (Gross & John, 2003).
3b	Report whether participants were provided with a strategy	They were then asked to use mental imagery to separately induce and intensify each of the four emotional states based on their own subjective experience, without receiving any specific imagery instructions beforehand.
3c	Report the strategies participants used	Additionally, we classified participants' reported emotion imagery strategies into three categories: autobiographical memory recall, imagined situations (i.e., events that did not actually happen or were fictional), and body-related sensations (i.e., awareness of current breathing or bodily feelings). The distribution of emotion imagery strategies across participants is provided in Supplementary Figure S7.
3d	Report methods used for online-data processing and artifact correction	Data was processed online using Turbo-BrainVoyager (TBV) version 4.2 (Brain Innovation B.V., Maastricht, The Netherlands) and imported in Python using the TBV Network Access Plugin and the corresponding interface (https://github.com/expyriment/expyriment-stash/) as part of the open-source Expyriment library. The rt-RSA Python tool, freely available at (https://github.com/assuntaciarlo/rtRSA_GUI), was used for pattern analysis and feedback display.
3e	Report condition and group effects for artifacts	*Condition and group effects for artifacts were not measured, or not reported in the manuscript*
Feedback specifications		
4a	Report how the online-feature extraction was defined	After all the four localizer runs, the rt-RSA tool was used to generate four base patterns by selecting voxels which were related to emotion imagination (univariate selection) and allowed semantic discernibility between emotions (multivariate selection). In the univariate selection, voxels were picked based on their absolute t-values, specifically those whose absolute t-values ranked within the top 60% to 90% of all the voxels within the defined emotion network. The multivariate selection first used a searchlight approach (with a spherical radius of 1 voxel) to generate a four-by-four representational dissimilarity matrix (RDM) for each voxel of the initial mask obtained from the univariate selection. This RDM encoded the dissimilarities between the four emotional patterns obtained from each searchlight, defined as one minus Pearson's correlation coefficient. Voxels were then selected if their RDMs achieved the top 5% similarity to a predefined model RDM, which treated emotions of opposing valence as maximally dissimilar while disregarding differences in arousal.
4b	Report and justify the reinforcement schedule	*The manuscript does not report or justify the reinforcement schedule*

4c	Report the feedback modality and content	The visual feedback provided information to the participants about two key aspects. First, the wedges of the target emotion thermometer were dynamically filled based on the intensity of the current brain activity pattern relative to the corresponding base pattern, extracted during the localizer runs. Second, the current activity pattern was represented as a moving red dot projected onto the CSM.
4d	Collect and report all brain activity variable(s) and/or contrasts used for feedback, as displayed to experimental participants	Three metrics were defined to evaluate neurofeedback performances, including (1) Pearson's correlation between the current brain activity pattern and the target base pattern, (2) angular distance between the moving red dot and the target emotion icon on the CSM, and (3) intensity level of the target emotion's thermometer on the CSM. Pearson's correlation implicitly measured the actual (dis)similarity between the current and target patterns, while angular distance and intensity level served as direct indicators of (dis)similarity and intensity for the participant. Intensity level exceeded zero only when the current pattern exhibited the highest similarity to the target base pattern.
4e	Report the hardware and software used	MR imaging data was acquired with a 3.0 Tesla Siemens MAGNETOM Prisma whole-body MRI system (Siemens Medical Solutions, Erlangen, Germany), equipped with a 20-channel head coil. Data was processed online using Turbo-BrainVoyager (TBV) version 4.2 (Brain Innovation B.V., Maastricht, The Netherlands) and imported in Python using the TBV Network Access Plugin and the corresponding interface (https://github.com/expyriment/expyriment-stash/) as part of the open-source Expyriment library. The rt-RSA Python tool, freely available at (https://github.com/assuntaciarlo/rtRSA_GUI), was used for pattern analysis and feedback display. The offline MRI data preprocessing was performed using fMRIPrep version 24.1.1 (ignored susceptibility distortion correction and slice timing correction; normalized to MNI152NLin2009cAsym, with 2 mm resolution). The following analysis, statistical tests and plotting relied on TBV and Python packages, including NumPy 1.19.2 (Harris et al., 2020), Pandas 1.1.5 (McKinney, 2010), SciPy 1.5.2 (Virtanen et al., 2020), Statsmodels 0.12.2 (Seabold & Perktold, 2010), Nilearn 0.9.2 (Abraham et al., 2014), NiBabel 4.0.2 (Brett et al., 2024), Matplotlib 3.3.4 (Hunter, 2007) and Seaborn 0.11.2 (Waskom, 2021).
Outcome measures - brain		
5a	Report neurofeedback regulation success based on the feedback signal	Here, we report the neurofeedback performance analysis for the emotion of joyful relaxation, as it was completed by the majority of participants in two consecutive runs, allowing for both within-run and between-run performance comparisons. Analysis of the optional third neurofeedback run targeting sadness, which was performed by fewer participants and included a single run, is provided in Supplementary Figure S3-S5 and Table S3-S7.
5b	Plot within-session and between-session regulation blocks of feedback variable(s), as well as pre-to-post resting baselines or contrasts	Additionally, as shown in Figure 4A, while correlations with the enthusiasm and anger patterns in the second run showed slight upward trends, all other non-target emotional patterns remained stable over time. In contrast, correlations with the joyful relaxation pattern increased in both runs. These results demonstrate a robust within-run learning effect, reflecting that participants were able to increasingly align their brain activity with the target pattern over time. This pattern suggests that participants seem to begin the second run with an improved baseline regulation ability, likely reflecting carryover from the first run. Overall, these results suggest a potential between-run learning effect, although the exploratory quadratic model adds greater complexity.
5c	Statistically compare the experimental condition/group to the control condition(s)/group(s) (not only each group to baseline measures)	*The manuscript does not statistically compare the experimental condition/group to the control condition(s)/group(s)*
Outcome measures - behaviour		
6a	Include measures of clinical or behavioural significance, defined a priori, and describe whether they were reached	Perceived control ratings demonstrated similar distributions across runs, with descriptive statistics (mean ± SD) of 4.64 ± 1.62 for the first run and 5.45 ± 2.28 for the second run. A paired t-test revealed no significant difference between runs ($t(21) = 1.80$, $p = 0.086$), although there was a trend toward higher ratings in the second run.
6b	Run correlational analyses between regulation success and behavioural outcomes	Furthermore, as shown in Figure 6, correlation analyses revealed a significant positive relationship between participants' perceived control ratings and their performance slopes for Pearson's correlation. In contrast, no significant relationships were observed for angular distance or intensity level. These findings were consistent across both neurofeedback runs, supporting the alignment between subjective reports and objective performance measures.
7a	Upload all materials, analysis scripts, code, and raw data used for analyses, as well as final values, to an open access data repository, when feasible	The rt-RSA Python tool, freely available at (https://github.com/assuntaciarlo/rtRSA_GUI), was used for pattern analysis and feedback display. The offline analysis scripts can be found at (https://github.com/xuelei-1021/rsanf). The data supporting the findings of this study will be made publicly available in a suitable repository at a later date.

This report has been generated using the CRED-nf online checklist version 1.0, adapted from the CRED-nf manuscript which is freely available here https://doi.org/10.1093/brain/awaa009.

Int. J. Neur. Syst. 2026.36. Downloaded from www.worldscientific.com
by 84.118.51.191 on 05/04/26. Re-use and distribution is strictly not permitted, except for Open Access articles.

Int. J. Neur. Syst. 2026.36. Downloaded from www.worldscientific.com
by 84.118.51.191 on 05/04/26. Re-use and distribution is strictly not permitted, except for Open Access articles.

ORCID

Xuelei Wang https://orcid.org/0000-0001-7350-3117
Assunta Ciarlo https://orcid.org/0000-0003-0683-2839
Michael Lührs https://orcid.org/0000-0002-5888-0843
Alexander Atanasyan https://orcid.org/0000-0002-7578-1820
David Böken https://orcid.org/0009-0007-9967-9728
Jürgen Roßmann https://orcid.org/0000-0002-8780-855X
Michael Schluse https://orcid.org/0000-0003-1336-2636
Maren Jäger https://orcid.org/0009-0000-2033-9560
Marisa Nordt https://orcid.org/0000-0001-5474-9314
Fengyu Cong https://orcid.org/0000-0003-0058-2429
Klaus Mathiak https://orcid.org/0000-0002-2276-7726
David E.J. Linden https://orcid.org/0000-0002-5638-9292
Rainer Goebel https://orcid.org/0000-0003-1780-2467
David M. A. Mehler https://orcid.org/0000-0001-6587-2617
Jana Zweerings https://orcid.org/0000-0002-5724-1054

References

1. R. Sitaram *et al.*, Closed-loop brain training: The science of neurofeedback, *Nat. Rev. Neurosci.* **18**(2) (2017) 86–100.
2. R. C. DeCharms, F. Maeda, G. H. Glover, D. Ludlow, J. M. Pauly, D. Soneji, J. D. Gabrieli and S. C. Mackey, Control over brain activation and pain learned by using real-time functional mri, *Proc. Natl. Acad. Sci. USA* **102**(51) (2005) 18626–18631.
3. P. Linhartová, A. Látalová, B. Kóša, T. Kašpárek, C. Schmahl and C. Paret, fmri neurofeedback in emotion regulation: A literature review, *NeuroImage* **193** (2019) 75–92.
4. V. Lorenzetti, B. Melo, R. Basílio, C. Suo, M. Yücel, C. J. Tierra-Criollo and J. Moll, Emotion regulation using virtual environments and real-time fmri neurofeedback, *Front. Neurol.* **9** (2018) 390.
5. F. Weiss, J. Zhang, A. Aslan, P. Kirsch and M. F. Gerchen, Feasibility of training the dorsolateral prefrontal-striatal network by real-time fmri neurofeedback, *Sci. Rep.* **12**(1) (2022) 1669.
6. N. Tschentscher, J. C. Tafelmaier, C. F. Woll, O. Pogarell, M. Maywald, L. Vierl, K. Breitenstein and S. Karch, The clinical impact of real-time fmri neurofeedback on emotion regulation: A systematic review, *Brain Sci.* **14**(7) (2024) 700.
7. D. M. Mehler *et al.*, Targeting the affective brain—a randomized controlled trial of real-time fmri neurofeedback in patients with depression, *Neuropsychopharmacology* **43**(13) (2018) 2578–2585.
8. K. D. Young, G. J. Siegle, V. Zotev, R. Phillips, M. Misaki, H. Yuan, W. C. Drevets and J. Bodurka, Randomized clinical trial of real-time fmri amygdala neurofeedback for major depressive disorder: Effects on symptoms and autobiographical memory recall, *Am. J. Psychiatry* **174**(8) (2017) 748–755.
9. J. Zweerings, K. Sarasjärvi, K. A. Mathiak, J. Iglesias-Fuster, F. Cong, M. Zvyagintsev and K. Mathiak, Data-driven approach to the analysis of real-time fmri neurofeedback data: Disorder-specific brain synchrony in ptsd, *Int. J. Neural Syst.* **31**(11) (2021) 2150043.
10. J. Zweerings *et al.*, Rt-fmri neurofeedback-guided cognitive reappraisal training modulates amygdala responsivity in posttraumatic stress disorder, *NeuroImage Clin.* **28** (2020) 102483.
11. J. Zweerings, E. M. Pflieger, K. A. Mathiak, M. Zvyagintsev, A. Kacela, G. Flatten and K. Mathiak, Impaired voluntary control in ptsd: Probing self-regulation of the acc with real-time fmri, *Front. Psychiatry* **9** (2018) 219.
12. A. A. Alegria *et al.*, Real-time f mri neurofeedback in adolescents with attention deficit hyperactivity disorder, *Hum. Brain Mapp.* **38**(6) (2017) 3190–3209.
13. S. Lukito *et al.*, Effects of fmri neurofeedback of right inferior frontal cortex on inhibitory brain activation in children with adhd, *Philos. Trans. R. Soc. B* **379** (1915) (2024) 20230097.
14. K. C. Kadosh, Q. Luo, C. de Burca, M. O. Sokunbi, J. Feng, D. E. Linden and J. Y. Lau, Using real-time fmri to influence effective connectivity in the developing emotion regulation network, *NeuroImage* **125** (2016) 616–626.
15. K. Shibata, T. Watanabe, M. Kawato and Y. Sasaki, Differential activation patterns in the same brain region led to opposite emotional states, *PLoS Biol.* **14** (9) (2016) e1002546.
16. R. M. Todd, V. Miskovic, J. Chikazoe and A. K. Anderson, Emotional objectivity: Neural representations of emotions and their interaction with cognition, *Annu. Rev. Psychol.* **71**(1) (2020) 25–48.
17. R. Lanzino, D. Avola, F. Fontana, L. Cinque, F. Scarcello and G. L. Foresti, Sateer: Subject-aware transformer for eeg-based emotion recognition, *Int. J. Neural Syst.* **35** (2025) 2550002.

Int. J. Neur. Syst. 2026.36. Downloaded from www.worldscientific.com
by 84.118.51.191 on 05/04/26. Re-use and distribution is strictly not permitted, except for Open Access articles.

18. X. Ping and W. Huang, Interactive eeg emotion recognition with incremental gaussian processes, *Int. J. Neural Syst.* **35** (2025) 2550041.
19. J. B. Ritchie, D. M. Kaplan and C. Klein, Decoding the brain: Neural representation and the limits of multivariate pattern analysis in cognitive neuroscience, *Br. J. Philos. Sci.* **70**(2) (2019) 581–607.
20. D. López-García, A. Sobrado, J. M. Peñalver, J. M. Górriz and M. Ruz, Multivariate pattern analysis techniques for electroencephalography data to study flanker interference effects, *Int. J. Neural Syst.* **30**(07) (2020) 2050024.
21. N. Kriegeskorte, M. Mur, D. A. Ruff, R. Kiani, J. Bodurka, H. Esteky, K. Tanaka and P. A. Bandettini, Matching categorical object representations in inferior temporal cortex of man and monkey, *Neuron* **60**(6) (2008) 1126–1141.
22. N. Kriegeskorte and R. A. Kievit, Representational geometry: Integrating cognition, computation, and the brain, *Trends Cogn. Sci.* **17**(8) (2013) 401–412.
23. J. Kolasinski, D. C. Dima, D. M. Mehler, A. Stephenson, S. Valadan, S. Kusmia and H. E. Rossiter, Spatially and temporally distinct encoding of muscle and kinematic information in rostral and caudal primary motor cortex, *Cereb. Cortex Commun.* **1**(1) (2020) tgaa009.
24. M. Nordt, J. Gomez, V. Natu, B. Jeska, M. Barnett and K. Grill-Spector, Learning to read increases the informativeness of distributed ventral temporal responses, *Cereb. Cortex* **29**(7) (2019) 3124–3139.
25. M. Nordt, J. Gomez, V. S. Natu, A. A. Rezai, D. Finzi, H. Kular and K. Grill-Spector, Longitudinal development of category representations in ventral temporal cortex predicts word and face recognition, *Nat. Commun.* **14**(1) (2023) 8010.
26. H. Kiyokawa and R. Hayashi, Commonalities and variations in emotion representation across modalities and brain regions, *Sci. Rep.* **14**(1) (2024) 20992.
27. R. Goebel, What's in the thermometer? towards semantic neurofeedback at 7 tesla, Chair's Symposium presented at Real-Time Functional Imaging and Neurofeedback (rtFIN) conference, (2019).
28. R. Goebel, Analysis methods for real-time fmri neurofeedback, *FMRI Neurofeedback* (Elsevier, 2021), pp. 23–55.
29. A. Ciarlo, A. G. Russo, S. Ponticorvo, F. Di Salle, M. Lührs, R. Goebel and F. Esposito, Semantic fmri neurofeedback: A multi-subject study at 3 tesla, *J. Neural Eng.* **19**(3) (2022) 036020.
30. A. G. Russo, M. Lührs, F. Di Salle, F. Esposito and R. Goebel, Towards semantic fmri neurofeedback: Navigating among mental states using real-time representational similarity analysis, *J. Neural Eng.* **18**(4) (2021) 046015.
31. R. Goebel, M. Lührs, A. Ciarlo, F. Esposito and D. E. Linden, Semantic fmri neurofeedback of emotions: From basic principles to clinical applications, *Philos. Trans. R. Soc. B* **379**(1915) (2024) 20230084.
32. E. Lescrauwaet, Semantic fMRI neurofeedback: From mechanisms to clinical applications, Master's thesis, Maastricht University (2021).
33. S. J. Fede, S. F. Dean, T. Manuweera and R. Momenan, A guide to literature informed decisions in the design of real time fmri neurofeedback studies: A systematic review, *Front. Hum. Neurosci.* **14** (2020) 60.
34. L. A. Feldman, Valence focus and arousal focus: Individual differences in the structure of affective experience, *J. Pers. Soc. Psychol.* **69**(1) (1995) 153.
35. J. Heffner and O. FeldmanHall, A probabilistic map of emotional experiences during competitive social interactions, *Nat. Commun.* **13**(1) (2022) 1718.
36. D. M. McNair *et al.*, Manual profile of mood states (1971).
37. J. J. Gross and O. P. John, Individual differences in two emotion regulation processes: Implications for affect, relationships, and well-being, *J. Pers. Soc. Psychol.* **85**(2) (2003) 348.
38. T. Ros *et al.*, Consensus on the reporting and experimental design of clinical and cognitive-behavioural neurofeedback studies (cred-nf checklist), *Brain* **143**(6) (2020) 1674–1685.
39. F. Krause and O. Lindemann, Expyriment: A python library for cognitive and neuroscientific experiments, *Behav. Res. Methods* **46**(2) (2014) 416–428.
40. K. A. Lindquist, T. D. Wager, H. Kober, E. Bliss-Moreau and L. F. Barrett, The brain basis of emotion: A meta-analytic review, *Behav. Brain Sci.* **35**(3) (2012) 121–143.
41. L. Skottnik and D. E. Linden, Mental imagery and brain regulation—new links between psychotherapy and neuroscience, *Front. Psychiatry* **10** (2019) 779.
42. A. Schaefer, R. Kong, E. M. Gordon, T. O. Laumann, X.-N. Zuo, A. J. Holmes, S. B. Eickhoff and B. T. Yeo, Local-global parcellation of the human cerebral cortex from intrinsic functional connectivity mri, *Cereb. Cortex* **28**(9) (2018) 3095–3114.
43. R. S. Desikan *et al.*, An automated labeling system for subdividing the human cerebral cortex on mri scans into gyral based regions of interest, *NeuroImage* **31**(3) (2006) 968–980.
44. S. Heunis *et al.*, The effects of multi-echo fmri combination and rapid t2*-mapping on offline and real-time bold sensitivity, *NeuroImage* **238** (2021) 118244.
45. K. Mathiak, A. Rapp, T. T. Kircher, W. Grodd, I. Hertrich, N. Weiskopf, W. Lutzenberger and H. Ackermann, Mismatch responses to randomized gradient switching noise as reflected by fmri and whole-head magnetoencephalography, *Hum. Brain Mapp.* **16**(3) (2002) 190–195.
46. Y. O. Halchenko *et al.*, Heudiconv—flexible dicom conversion into structured directory layouts, *J. Open Source Softw.* **9**(99) (2024) 5839.
47. O. Esteban *et al.*, fmriprep: A robust preprocessing pipeline for functional mri, *Nat. Methods* **16**(1) (2019) 111–116.

Int. J. Neur. Syst. 2026.36. Downloaded from www.worldscientific.com
by 84.118.51.191 on 05/04/26. Re-use and distribution is strictly not permitted, except for Open Access articles.

48. O. Esteban *et al.*, Analysis of task-based functional mri data preprocessed with fmriprep, *Nat. Protoc.* **15** (7) (2020) 2186–2202.
49. C. R. Harris *et al.*, Array programming with numpy, *Nature* **585**(7825) (2020) 357–362.
50. W. McKinney *et al.*, Data structures for statistical computing in python, *SciPy* **445**(1) (2010) 51–56.
51. P. Virtanen *et al.*, Scipy 1.0: Fundamental algorithms for scientific computing in python, *Nat. Methods* **17** (3) (2020) 261–272.
52. S. Seabold *et al.*, Statsmodels: Econometric and statistical modeling with python, *SciPy* **7**(1) (2010) 92–96.
53. A. Abraham, F. Pedregosa, M. Eickenberg, P. Gervais, A. Mueller, J. Kossaifi, A. Gramfort, B. Thirion and G. Varoquaux, Machine learning for neuroimaging with scikit-learn, *Front. Neuroinform.* **8** (2014) 14.
54. M. Brett *et al.*, NiBabel (2022).
55. J. D. Hunter, Matplotlib: A 2d graphics environment, *Comput. Sci. Eng.* **9**(03) (2007) 90–95.
56. M. L. Waskom, Seaborn: Statistical data visualization, *J. Open Source Softw.* **6**(60) (2021) 3021.
57. Y. Behzadi, K. Restom, J. Liau and T. T. Liu, A component based noise correction method (compcor) for bold and perfusion based fmri, *NeuroImage* **37**(1) (2007) 90–101.
58. E. T. Rolls, C.-C. Huang, C.-P. Lin, J. Feng and M. Joliot, Automated anatomical labelling atlas 3, *NeuroImage* **206** (2020) 116189.
59. J. C. Gower, Some distance properties of latent root and vector methods used in multivariate analysis, *Biometrika* **53**(3–4) (1966) 325–338.
60. W. S. Torgerson, Theory and methods of scaling (1958).
61. C. Paret, N. Goldway, C. Zich, J. N. Keynan, T. Hendler, D. Linden and K. C. Kadosh, Current progress in real-time functional magnetic resonance-based neurofeedback: Methodological challenges and achievements, *NeuroImage* **202** (2019) 116107.
62. N. Weiskopf, F. Scharnowski, R. Veit, R. Goebel, N. Birbaumer and K. Mathiak, Self-regulation of local brain activity using real-time functional magnetic resonance imaging (fmri), *J. Physiol. Paris* **98**(4–6) (2004) 357–373.
63. A. R. Barreiros, I. Almeida, B. C. Baía and M. Castelo-Branco, Amygdala modulation during emotion regulation training with fmri-based neurofeedback, *Front. Hum. Neurosci.* **13** (2019) 89.
64. S. Johnston, D. E. J. Linden, D. Healy, R. Goebel, I. Habes and S. Boehm, Upregulation of emotion areas through neurofeedback with a focus on positive mood, *Cogn. Affect. Behav. Neurosci.* **11**(1) (2011) 44–51.
65. I. Habes, S. C. Krall, S. Johnston, K. Yuen, D. Healy, R. Goebel, B. Sorger and D. E. J. Linden, Pattern classification of valence in depression, *NeuroImage Clin.* **2** (2013) 675–683.
66. J. V. Haxby, Multivariate pattern analysis of fmri: The early beginnings, *NeuroImage* **62**(2) (2012) 852–855.
67. A. Mahmoudi, S. Takerkart, F. Regragui, D. Boussaoud and A. Brovelli, Multivoxel pattern analysis for fmri data: A review, *Comput. Math. Methods Med.* **2012**(1) (2012) 961257.
68. J. F. Sima, H. Schultheis and T. Barkowsky, Differences between spatial and visual mental representations, *Front. Psychol.* **4** (2013) 240.
69. M. Wicken, R. Keogh and J. Pearson, The critical role of mental imagery in human emotion: Insights from fear-based imagery and aphantasia, *Proc. R. Soc. B* **288**(1946) (2021) 20210267.
70. L. Alexander, C. M. Wood and A. C. Roberts, The ventromedial prefrontal cortex and emotion regulation: Lost in translation? *J. Physiol.* **601**(1) (2023) 37–50.
71. V. Menon and L. Q. Uddin, Saliency, switching, attention and control: A network model of insula function, *Brain Struct. Funct.* **214**(5) (2010) 655–667.
72. M. A. Frost and R. Goebel, Functionally informed cortex based alignment: An integrated approach for whole-cortex macro-anatomical and roi-based functional alignment, *NeuroImage* **83** (2013) 1002–1010.
73. J. V. Haxby, J. S. Guntupalli, S. A. Nastase and M. Feilong, Hyperalignment: Modeling shared information encoded in idiosyncratic cortical topographies, *eLife* **9** (2020) e56601.
74. S. Berboth, C. Windischberger, N. Kohn and C. Morawetz, Test-retest reliability of emotion regulation networks using fmri at ultra-high magnetic field, *NeuroImage* **232** (2021) 117917.
75. C. L. Nord, A. Gray, C. J. Charpentier, O. J. Robinson and J. P. Roiser, Unreliability of putative fmri biomarkers during emotional face processing, *NeuroImage* **156** (2017) 119–127.
76. S. Noble, D. Scheinost and R. T. Constable, A guide to the measurement and interpretation of fmri test-retest reliability, *Curr. Opin. Behav. Sci.* **40** (2021) 27–32.
77. F. Portal, J. De Lope and M. Graña, A performance benchmarking review of transformers for speaker-independent speech emotion recognition, *Int. J. Neural Syst.* **35**(10) (2025) 2530001.